UNIVERSITY OF TARTU

INSTITUTE OF ECOLOGY AND EARTH SCIENCES

DEPARTMENT OF GEOLOGY

Marian Külaviir

Secondary changes in Palaeoproterozoic Zaonega Formation carbonate rocks in Onega Parametric Hole, Karelia, Russia

MSc thesis

Suprevisor: Kalle Kirsimäe

Aivo Lepland

TARTU 2016

Secondary changes in Palaeoproterozoic Zaonega Formation carbonate rocks in Onega Parametric Hole, Karelia, Russia

The isotopic composition of carbonate rocks and organics in Zaonega Formation has been widely used to study, the global carbon cycle. However the carbonate rocks of Zaonega Fm. are affected by fluidal and/or metamorphic processes that have significantly altered their isotopic composition. That emphasizes the importance of distinguishing primary versus secondary isotopic compositions in studies where carbonate rocks are used for reconstruction of global environmental change. The thesis aims for characterization of the mineral-isotopic composition of Zaonega Fm. in Onega Parametric drillhole and revealing the processes and mechanisms of the secondary alteration, its extent in different parts of the succession and finding if unaltered isotopic signal is present in some parts of the studied section. Combined mineralogical, petrographic and geochemical study of carbonate rocks reveals complex secondary alteration mechanism. Post-depositional magmatic or hydrothermal ^{13}C and ^{18}O depleted fluids carrying silica interacted with the initial carbonate phase, resulting in precipitation of ^{13}C and ^{18}O depleted secondary phases. Most probable source of ^{13}C-depleted DIC were products of decomposition/oxidation of organic material with $\delta^{13}C$ between –25 and –42 ‰. Interaction between silica and dolomite is seen at the margins of carbonate beds and is associated with formation of calcite, authigenic quarz and different phyllosilicate minerals such as talc and mica (calcite ± talc ± phlogopite ± actinolite paragenesis). Non-linear co-variation between $\delta^{13}C_{carb}$ and $\delta^{18}O_{carb}$ values are compared with Jacobsen and Kaufman (1999) mass-balance model, revealing at least three fluid-rock interaction episodes.

Zaonega, Onega Parametric Hole, carbonate rocks, carbon isotopes, oxygen isotopes

P420 Petrology, mineralogy, geochemistry

Sekundaarsed muutused Paleoproterosoikumi Zaonega kihistu karbonaatsetes kivimites Onega parameetrilises puuraugus, Karjalas Venemaal

Karbonaatsete kivimite isotoopset koostist Zaonega kihistus on laialdaselt uuritud Paleoproterosoikumi süsinikuringe rekonstrueerimiseks. Zaonega kihistu kivimite algne isotoopne koostis on oluliselt mõjutatud fluidide ja moondeprotsesside poolt, seetõttu on globaalsete keskkonnamuutuste rekonstrueerimisel oluline eristada karbonaatkivimite algset ja sekundaarset isooopkoostist. Selle töö eesmärgiks on Onega parameetrilise puuraugu Zaonega

kihistu karbonaatkivimite mineraloogilise ja isotoopse koostise kirjeldamine, sekundaarsete protsesside, nende mehhannismide ja ulatuse esile toomine ning võimalikult primaarse isotoopsignaali leidmine uuritavas intervallis. Mineraloogiliste, petrograafiliste ja geokeemiliste analüüside tulemusena leiti, et kompleksse sekundaarse protsessi tulmusena on algse kivimi koostis muutunud. Muutumine on toimunud ^{13}C-ja ^{18}O-vaesete, ränidioksiidi sisaldavate magmaliste või hüdrotermaalsete fluidide toimel. Fluidi reageerimisel kivimiga tekkisid ^{13}C-ja ^{18}O-vasustunud sekundaarsed karbonaatsed faasid. Kõige tõenäolisemalt olid ^{13}C-vaesed ühendid pärit orgaanilise materjali lagunemisest/oksüdeerumisest. Ränidioksiidi ja dolomiidi reaktsioonil tekkisid kaltsiit, autigeenne kvarts ja kihtsilikaadid, neid mineraale on kõige rohkem näha karbonaatkivimi kihtide äärealadel. Võrreldes $\delta^{13}C_{carb}$ ja $\delta^{18}O_{carb}$ graafikut Jacobseni ja Kaufmani (1999) massitasakaalu mudeliga on näha, et peale settimist on Zaonega kihistu karbonaatkivimid erineva koostisega fluididega reageerinud vähemalt kolmel erineval korral.

Zaonega, Onega parameetriline puurauk, karbonaatsed kivimid, süsiniku isotoobid, hapniku isotoobid

P420 Petroloogia, mineraloogia, geokeemia

Table of Contents

Introduction

Stable carbon isotope ratios in carbonate sedimentary rocks (limestones and/or dolostones) are widely used for reconstructing the global carbon cycle and associated environmental conditions as far back in Earth's history as the sedimentary rock record exists. It is assumed that carbon isotopes track the balance between organic carbon burial and weathering. Fluctuations in carbon isotopic record archived in carbonate rocks throughout the Earth's history are usually small ($\delta^{13}C$ values varying ±5 ‰) and short-lived (<20 Myr), this is why Earth's carbon cycle is considered relatively stable (Schidlowski, 2001). However, this relatively stable carbon isotope record has been disrupted by several global large-scale C-isotope perturbations (Lyons *et al.*, 2014). One of the very first events and the most prominent of them, the Lomagundi-Jatuli event, took place in Palaeoproterozoic ca. 2.3-2.0 Ga (Baker and Fallick, 1989a; Karhu and Holland, 1996), right after the Great Oxygenation Event (GOE) at ca 2.4 Ga (Bekker *et al.*, 2004) and is globally recognized in carbonate sedimentary formations of that time (Baker and Fallick, 1989a, b; Karhu, 1993; Buick *et al.*, 1998; Bekker *et al.*, 2006).

The anomalous ^{13}C enriched carbon isotope composition of marine carbonates during the Lomagundi excursion is most probably tied to intensified burial of organic matter (Karhu and Holland, 1996). However, also diagenetic carbonate precipitation/recrystallization has been proposed as explaining the high $\delta^{13}C$ values (Hayes and Waldbauer, 2006). Nevertheless, there is an established consensus that Lomagundi excursion is caused by organic carbon burial, which in turn indicates that oxygen concentration in atmosphere could have been 12 to 22 times higher than present atmospheric level (PAL, Karhu and Holland, 1996). It is particularly interesting that first massive organic rich sediments appear world-wide roughly in the same time interval where Lomagundi-Jatuli excursion is dated (e.g. Ivankin *et al.*, 1987; Crick *et al.*, 1988; Premovic *et al.*, 1988).

One of the most prominent accumulations of organic-rich sediments with C_{org} content >40 wt % occurs in the Zaonega Formation of Onega Basin, Karelia, NW Russia (Melezhik *et al.*, 1999; Melezhik *et al.*, 2004). Age of the Zaonega Formation is constrained between 1975.3±2.8 and 1967.6±3.5 Ma (Martin *et al.*, 2015) which indicates its formation right after the Lomagundi-Jatuli excursion when $\delta^{13}C$ values were decreasing to normal marine values around 0 ‰ (Karhu, 1993)

The Zaonega succession is composed of mixed, organic rich siliciclastic-carbonate sediments intersected by numerous syndepositional mafic lavas and sills, indicating a rift basin

depositional environment on an active continental margin (Črne *et al.*, 2013a, b; Melezhik *et al.*, 2013). The isotopic composition of carbonate rocks and organics in Zaonega Formation has been widely used to study, in comparison with other sections of this time, the global carbon cycle (e.g., Melezhik *et al.*, 1999; Kump *et al.*, 2011).

However, recently Črne and others (2014) did show that the carbonate rocks of Zaonega Formation are affected by fluidal and/or metamorphic processes that have significantly altered their isotopic composition. That emphasizes the importance of distinguishing primary versus secondary isotopic compositions in studies where carbonate rocks are used for reconstruction of global environmental change.

In this thesis I undertook a detail petrographic, mineralogical and isotope geochemical study of the carbonate deposits of Zaonega Formation revealed in Onega Parametric Drillhole which is located in the central part of the Onega Basin (Figure 1).

The thesis aims for characterization of the mineral-isotopic composition of these carbonate beds and revealing the processes and mechanisms of the secondary alteration, its extent in different parts of the succession and finding if unaltered isotopic signal is present in some parts of the studied section.

Geological setting

Zaonega Formation is a part of the Palaeoproterozoic sedimentary succession in Onega basin, which is located in southeastern part of the Palaeoproterozoic Karelian craton and on the southeastern margin of the Baltic Shield in North-West Russia (Figure 1). Onega basin is filled with a sequence of greenschist metamorphic-grade volcano-sedimentary rocks unconformably lying on Archean granites and gneisses. The succession dips 10-50 ° filling a large, NW-SE-trending synform, which is diving under Palaeozoic sedimentary rocks south of Lake Onega. During the Svecofennian orogeny at 1.89-1.79 Ga the Palaeoproterozoic strata underwent deformation and greenschist-facies metamorphism (see Melezhik and Hanski, 2013 for in depth overview).

The succession of the Onega Basin is subdivided into eight formations: Glubokozero, Kumsa, Paljozero, Jangozero Medvezhegorsk, Tulomozero, Zaonega and the Suisari Formation (Melezhik and Hanski, 2013). The Zaonega sequence lies on the Tulomozero Formation, where carbonate rocks are characterized by positive carbon isotope signature known as Lomagundi-Jatuli Isotopic Event (LJIE) (Karhu and Holland, 1996). Of all the formations in Onega basin, Zaonega has the largest areal distribution and it is known to be a record of Shunga event – an intensive accumulation of organic material after the occurrence of LJIE (e.g., Kump *et al.*, 2011)

There has been some controversy in determining the age of Zaonega Formation. The maximum age of the Zaonega Formation is constrained by the underlying Burakovka Pluton dated at 2449 ± 1 Ma (Amelin *et al.*, 1995). However, others have proposed that Zaonega Formation is younger than 2050 Ma (Hannah *et al.*, 2008; Ovchinnikova *et al.*, 2007); younger than 2058.6 ± 0.8 Ma (Martin *et al.*, 2013; Melezhik *et al.*, 2007) or younger than 1975.3 ± 2.8 (Martin *et al.*, 2015). Recently, Martin and others (2015) suggested that the age of Zaonega Formation is bracketed between 1975.3 ± 2.8 and 1967.6 ± 3.5 Ma.

Zaonega Formation is composed of sedimentologically immature siliciclastic rocks, mudstones, cherts and dolostones with abundant tuffs, lavas and sills intersecting or interlayering those, suggesting to an intraplate rift associated with high volcanic and hydrothermal activity (Črne *et al.*, 2013a). The sediments accumulated with elevated sedimentation rate in a nutrient rich, non-euxinic, brackish-water, possibly in lagoonal environment whereas the redox conditions at the sediment-water interface show fluctuating oxic-suboxic/anoxic behavior during the deposition of Zaonega sediments (Asael *et al.*, 2013). During the formation of Zaonega succession the magmatic bodies present in the section were presumably intruded into wet, unconsolidated

sediments, thus triggering hydrothermal circulation (Črne *et al.,* 2013a, b). Hydrothermal activity initiated hydrocarbon formation and migration arguably forming one of the earliest petroleum deposits on Earth (Črne *et al.,* 2013a; Melezhik *et al.,* 1999). Due to accumulation of C_{org} and the hydrocarbon migration the sedimentary rocks of Zaonega Formation host at least several weight percent of organic carbon (autochtonous kerogen residues and allochtonous pyrobitumen), with many highly-enriched layers which can contain up to 98 wt % of organic carbon. (Melezhik *et al.*, 1999; Črne *et al.,* 2013a, b)

The hydrocarbons in Zaonega Formation are biogenic in origin, most likely formed during catagenesis from accumulated remnants of algae or bacteria. The carbon isotope composition of organic material is highly variable with $\delta^{13}C_{org}$ values between –45 ‰ to –17 ‰, referring to complex catagenetic and metamorphic alteration of the original material, whereas it is suggested that carbon isotope signature in initial biomass was of –34 ‰ (Melezhik *et al*., 1999). Seepage of hydrocarbons onto seafloor potentially provided habitats for methane metabolizing microbial communities also contributing to shifting of biomass $\delta^{13}C_{org}$ to more depleted values (Qu *et al.*, 2012. Likewise the range of $\delta^{13}C_{carb}$ values of –5 to –26 ‰ in carbonates associated with organic material are considered to have been changed from their Palaeoproterozoic values by post-depositional processes (Melezhik *et al.*, 1999).

Carbonate rocks in Zaonega succession occur as massive rock. Melezhik and others (1999) characterized two lithological types: (a) massive structureless, lensoidal, fine- to medium-grained, black and organic carbon rich secondary rocks were classified as dolostone megaconcretions; (b) lensoidal or thin beds, primary laminated, grey organic carbon poor or black organic carbon rich, were classified as sedimentary dolostones. Alternatively a study by Črne and others (2013a) proposed that massive dolostone was formed during recrystallization and the dolostone megaconcretions were the outcome of sedimentary, diagenetic, hydrothermal, metasomatic or multigenetic processes.

The carbonate beds in the Zaonega Formation are interbedded and/or intersected by mudstone and chert beds/lenses. The chert in Zaonega Formation appears as a black, massive rock with a conchoidal fracture. It was described by Melezhik and others (1999) as a cloudy textured chert with a fine crystalline groundmass exhibiting no lamination, and possibly as a primary siliceous chemical sediment. However, Črne and others (2013b) and Üpraus (2014) have suggested that massive chert is of secondary origin evidencing the post-depositional mobilization of silica.

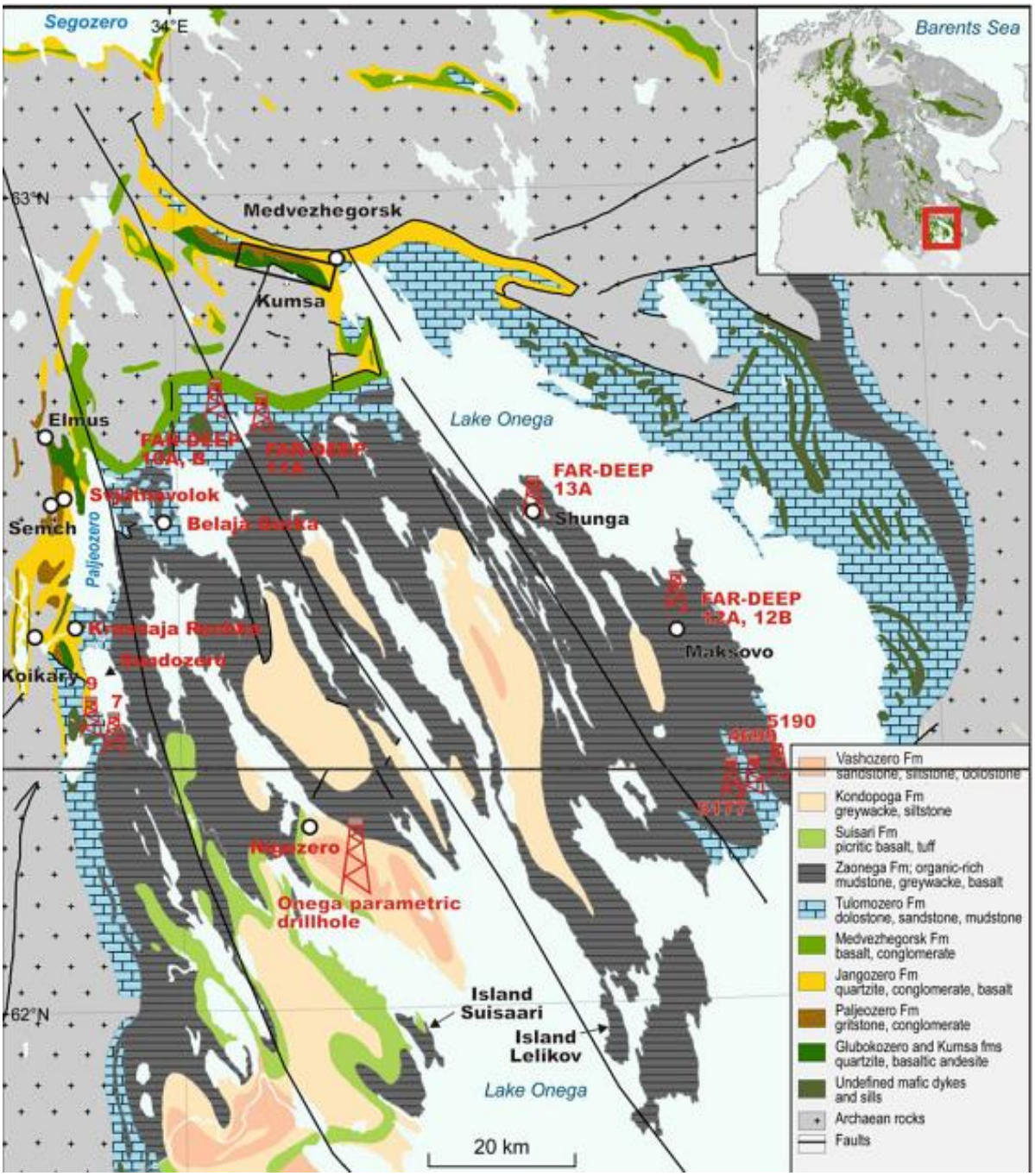

Figure 1. Geological map of the Onega basin, Karelia, Russia showing locations of drillholes (from Melezhik *et al.*, 2013).

Materials and methods

Organic-rich carbonate rock samples were collected from Zaonega Formation in Onega Parametric drillcore (OPH; Figure 1, 2). The 3537 meters deep Onega Parametric drillhole (62.1 °N, 34.5 °E) was made in the northwestern part of the Palaeoproterozoic Onega structure in 2008 by Institute of Geology, Karelian Centre of Russian Academy of Sciences. The hole extends through 2944 meters thick volcanic sedimentary succession down to Archean granite-greenstone basement (Glushanin *et al.*, 2011).

The samples for mineralogical and isotopic analysis were obtained from four carbonate beds in upper part of the Zaonega Formation using a minidrill. At contacts between carbonate rock with other rock layers (mudstone, chert) the samples were taken more closely than in the interior of the carbonate rock layer (Figure 3). Altogether 116 powder samples between depths 1103.59 m and 1123.20 m, were collected. Also 7 rock slabs perpendicular to bedding were taken from the same interval for preparing thin sections for microscopic analysis with scanning electron microscope.

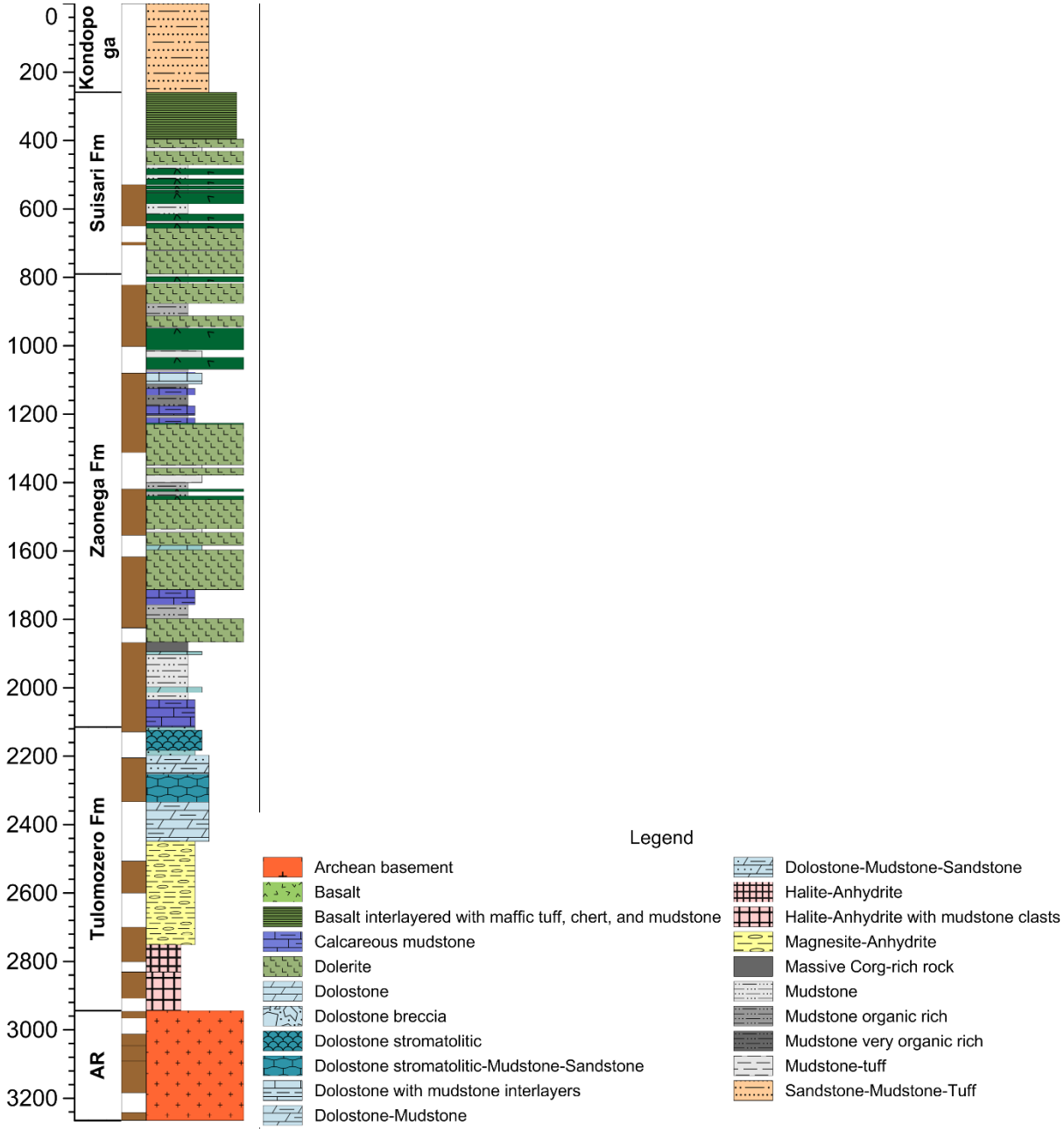

Figure 2. Lithostratigraphic column of Onega Parametric drillhole (Kärt Üpraus, personal communication 2016).

The mineralogical compositions of whole rock samples was studied by means of X-ray diffractometry (XRD). Samples were pulverized in a planetary mill and unoriented preparations were made. Preparations were scanned on Bruker D8 Advance diffractometer using Cu *K*α radiation and LynxEye positive sensitive detector in 2-70 ° 2-Theta range. The quantitative mineralogical composition of the samples was interpreted and modelled by using the Rietveld algorithm-based program Topaz.

From 500 micrograms of powdered dolostone, carbon and oxygen stable isotope ratios in carbonates ($\delta^{13}C_{carb}$, $\delta^{18}O_{carb}$) were measured by isotope-ratio mass spectrometry (IRMS) using Thermo Delta V Advance mass-spectrometer with GAS-Bench II interface. The results are reported respective to VPDB standard in per mil.

In order to measure stable carbon isotope ratio in organic material present in all samples 10 % HCl was used to dissolve all carbonates interfering with carbon isotope signal in organic material. After removing of carbonates the retained organic material was rinsed multiple times, dried and weighed for analysis with Delta V Plus mass-spectrometer with Flash HT Plus interface. The C_{org} isotope composition is reported respective to VPDB standard in per mil.

The thin sections made out of the slabs taken during sampling were studied using scanning electron microscope (SEM) analysis. SEM imaging of carbon coated samples was done using a ZEISS EVO MA15 SEM. The images were captured by backscattered electron mode and chemical characterization by elemental mapping of the samples was carried out with Oxford AZTEC-MAX energy-dispersive spectroscopy (EDS) attached to SEM.

Time-of-Flight Secondary Ion Mass Spectrometry (TOF-SIMS) was performed using ULVAC-PHI Inc. PHI TRIFT V nanoTOF to map elemental composition and measure isotopic composition of carbonate minerals. TOF-SIMS is a type of mass spectrometric method where atoms and molecules in the sample are ionized, the stream of ions is sent through a mass analyser which separates ions based on their mass-to-charge ratio (m/z), then for each m/z, the number of ions is counted and compared with a standard which allows for the quantification od the analyte in the sample. In case of TOF-SIMS the ionization is carried through with an instrument where an ion beam (Ga^+, Ar^+, Cs^+, N_2^+ or O_2^+) interacts with a solid, causing the solid to emit secondary ions which are collected into a beam that goes into the mass analyser. The ionizing ion beam can be focused down to 70-100 nm, allowing for very detailed surface analyses. Mass analyser of TOF-SIMS instrument measures the time when an accelerated particle with specific velocity reaches the detector. Particles with various m/z ratios acquire different velocities enabling the time specific separation. TOF-SIMS enables very detailed elemental analysis and mapping of surface, where every pixel of a TOF-SIMS map represents a full mass spectrum (Benninghoven *et al.*, 1987).

Figure 3. Example of a dolostone-mudstone/chert contact in OPH core (depth 1115.39 m). Red dots indicate location of mini-drilled samples. Sampling density was higher at dolomite-mudstone/chert contacts.

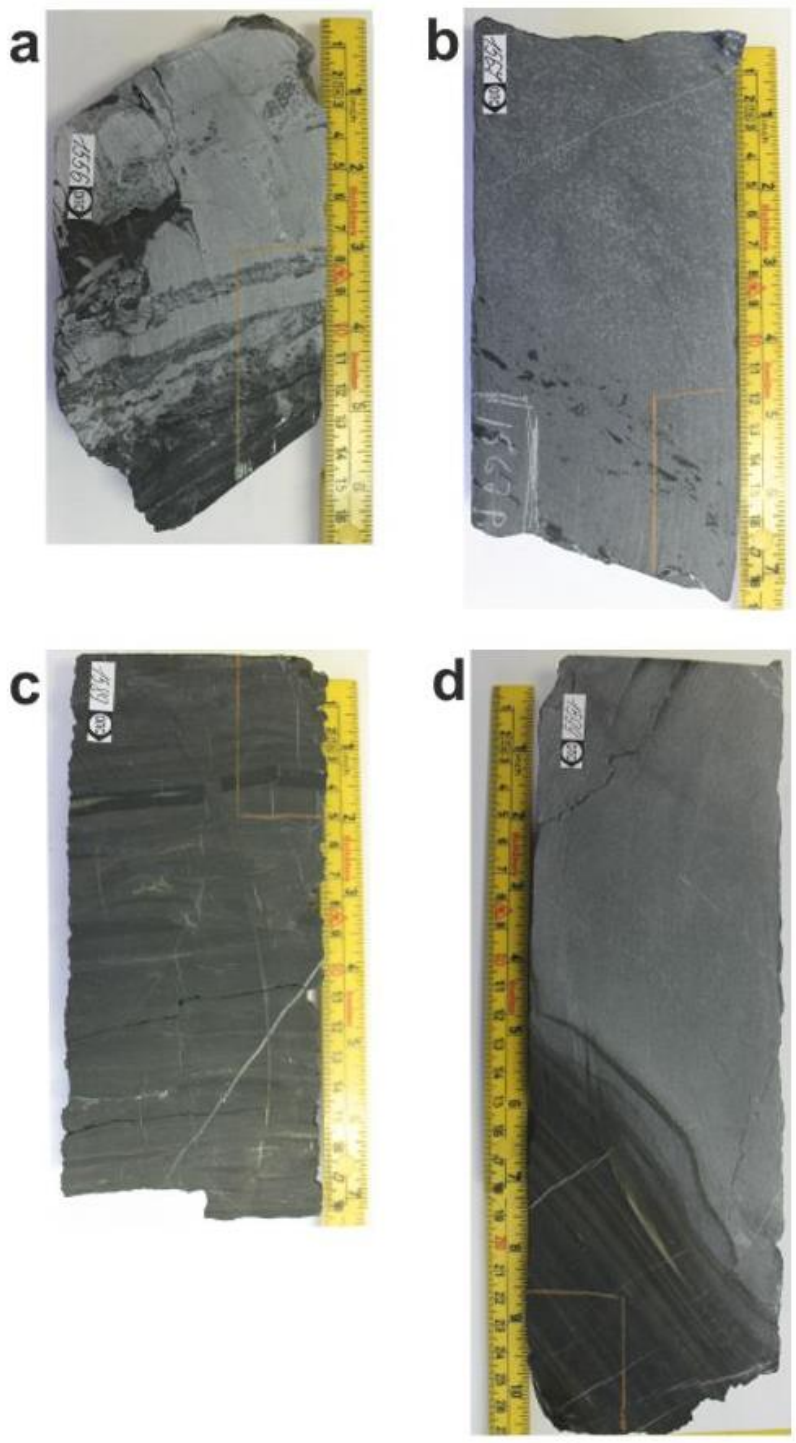

Figure 4. Main rock types in sampled intervals: a) carbonate rock interlayered with mudstone and chert; b) indistinctly bedded carbonate rock with some distinctive phosphate rich layers; c) layered organic rich mudstone; d) contact between laminated mudstone and carbonate rock.

Results

Using detailed sampling, geochemical and mineralogical characterization was aimed: (i) to find the distribution of carbonate phases with respect to contact zones; (ii) to determine the carbon and oxygen isotope composition in relation to minerals and contact zones; (iii) to observe the distribution of different mineral phases inside the dolostone layers.

X-ray diffraction

Whole-rock mineral composition of analyzed samples is shown in Table 1 in Appendix and in Figures 5, 6 and 7. Mineral composition of the studied carbonate rocks is characterized by dolomite and calcite composition at highly varying proportions. The dolomite content varies from trace amounts (<0.5 wt %) to 93.6 wt % of crystalline phases, and content of calcite ranges from 1.1 to 83 wt % (Table 1, Figure 6, 7). Calcite is the predominant phase at and close to contacts to mudstone and chert beds whereas dolomite is practically absent at margins of carbonate layers and its content is the highest in the interior/middle parts of the carbonate beds (Figure 7). There is a clear negative trend between dolomite and calcite (Figure 8) suggesting that these phases replace themselves in carbonate beds, though calcite can occur in mudstone and chert beds enclosing the carbonate layers as well.

Content of quartz and to some extent also K/Mg-mica is, similar to calcite, higher at the margins of the carbonate layers varying from 0.1 to 52.7 wt % and 1.5 to 86.7 wt %, respectively. K-feldspar and plagioclase content in carbonate layers varies from 0.2 to approximately 3 wt % for both phases and their content does not show clear dependence on the position with respect to the margins of carbonate beds (Figure 7). Talc was identified in three carbonates beds out of four sampled in OPH core and its content reached up to 15.8 wt % of crystalline phases. Talc occurs in these beds at their margins together with calcite, but predominantly at the lower portions/contacts of these three carbonate beds, which is clearly evident in two upper carbonate horizons (Figure 7, 8).

In addition, carbonate-fluor apatite was commonly found in all carbonate horizons (up to 6.1 wt %, average 0.9 wt %) and also pyrite (Figure 6). Pyrite content varies between trace amounts (<0.5 wt %) to 10.8 wt %, but its content is markedly higher in two deeper carbonate horizons studied here (Figure 6). Also trace amounts of siderite and chlorite were occasionally detected (Figure 6).

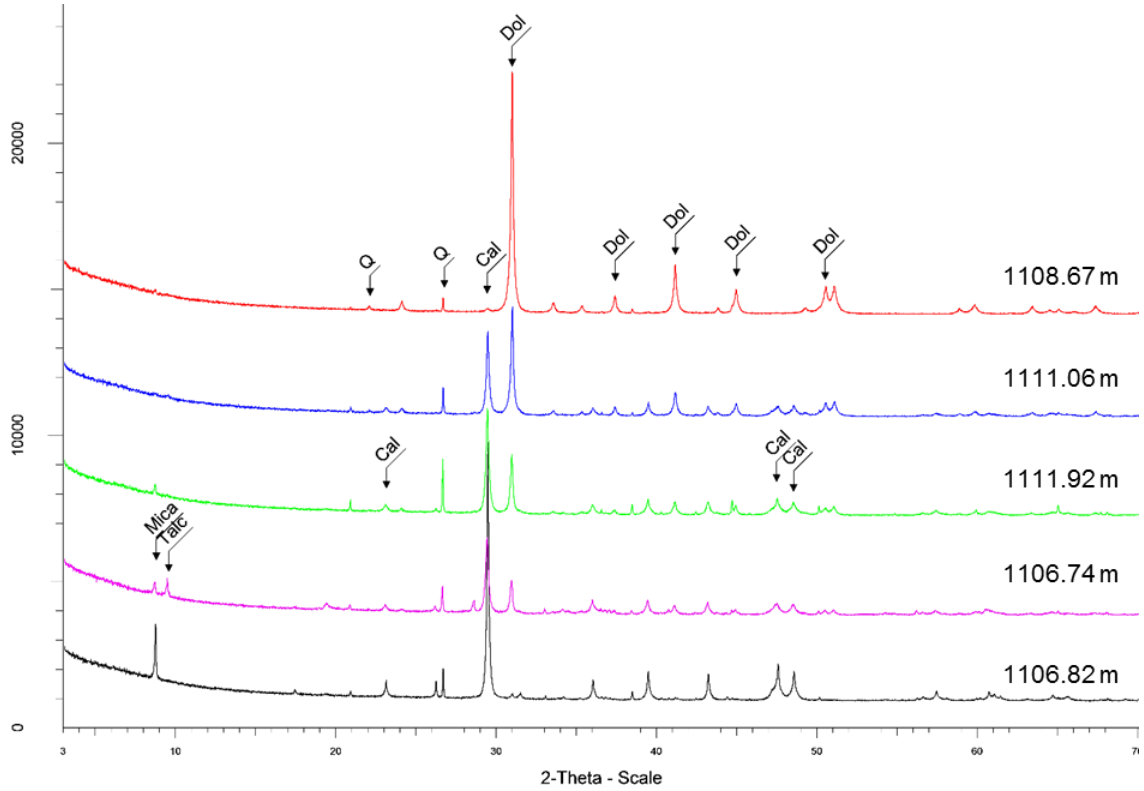

Figure 5. Examples of XRD spectra of carbonate rocks where dolomite content is increasing upwards.

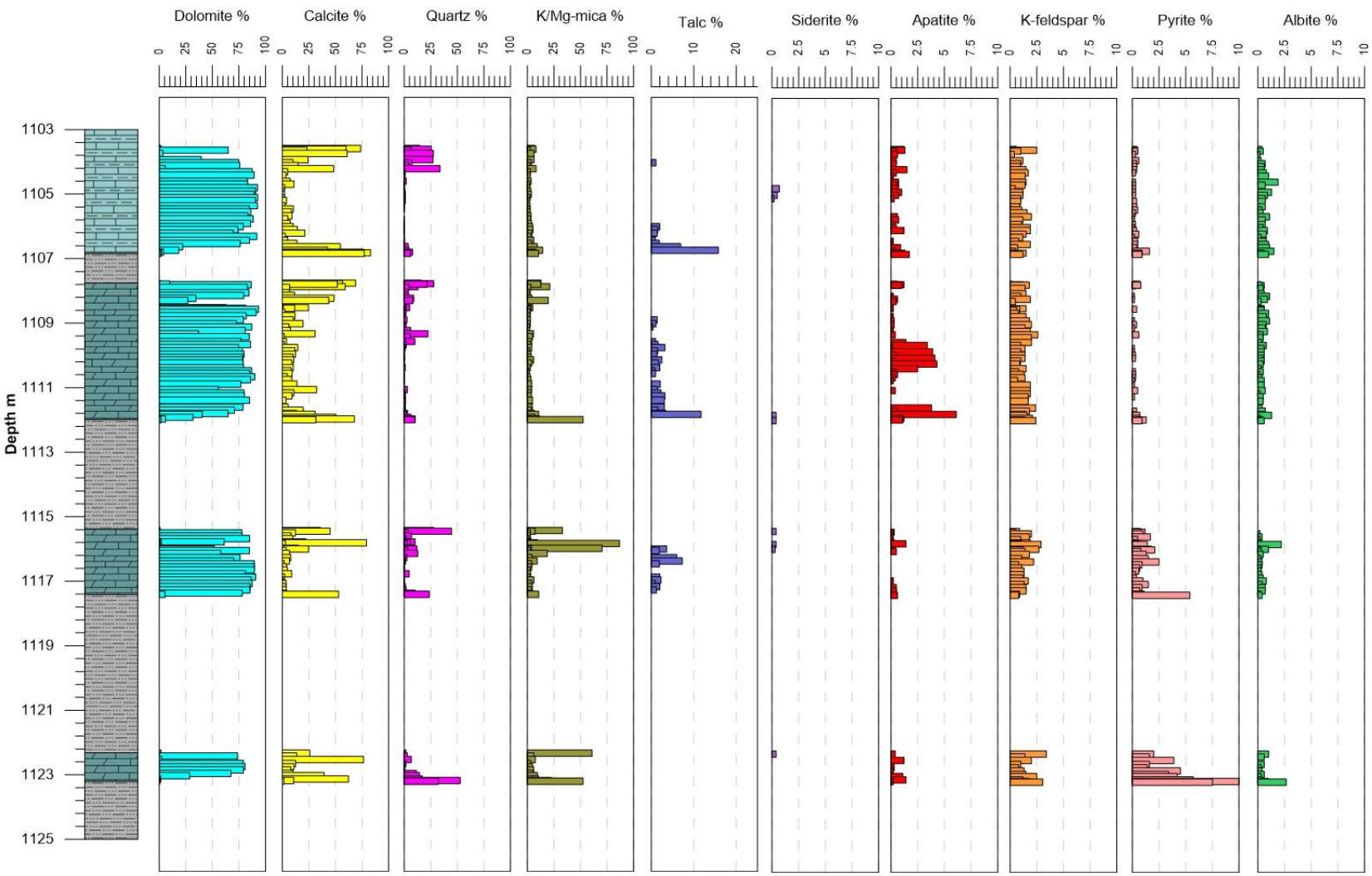

Figure 6. Simplified lithostratigraphic column (light blue represents dolostone with thin mudstone interlayers, blue represents dolostone and grey mudstone/chert) and mineralogy of the studied samples.

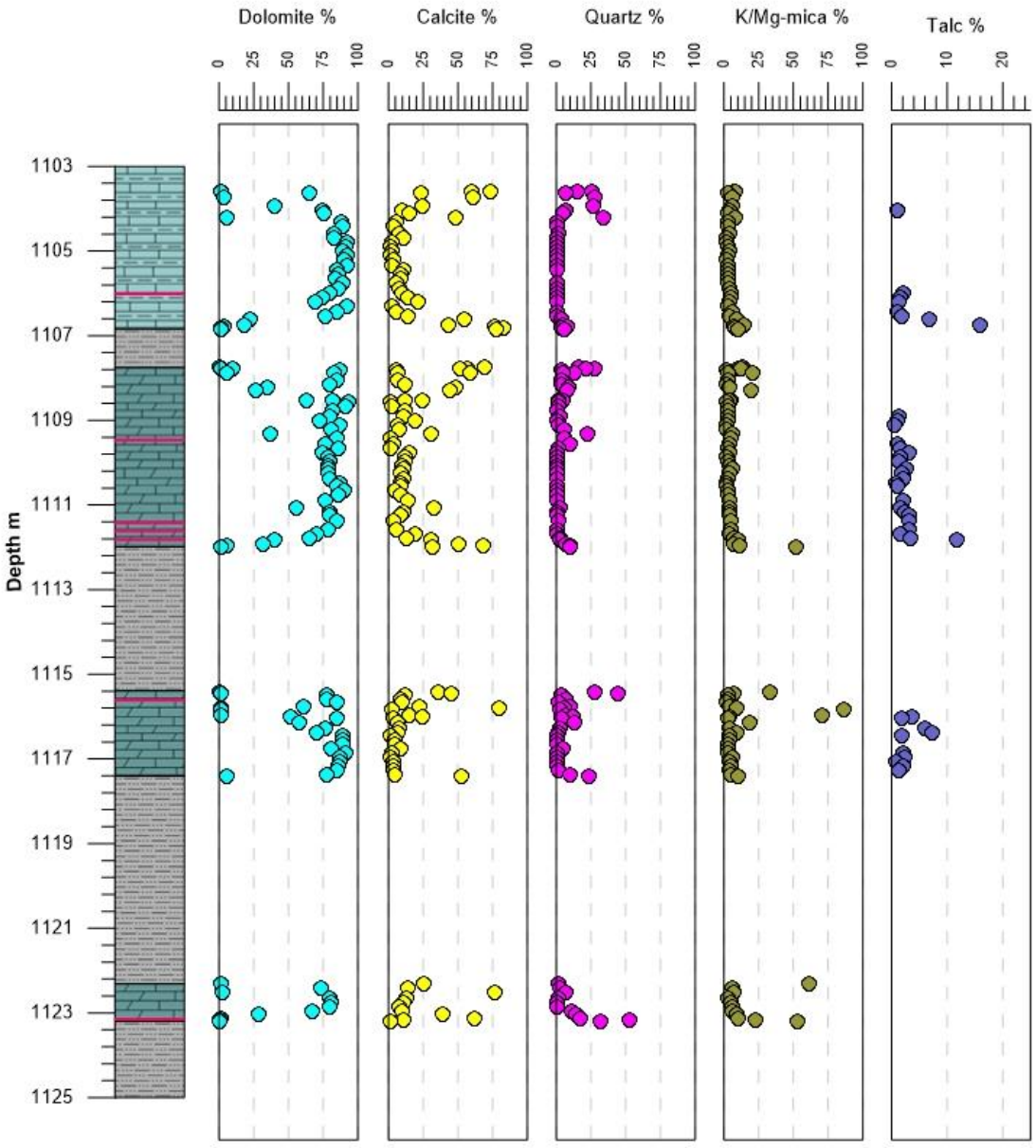

Figure 7. Variation of major mineral phases with the depth and in relation to carbonate rock beds, pink lines on lithostratigraphic column mark the depths of thin sections (see chapter Electron microscopy).

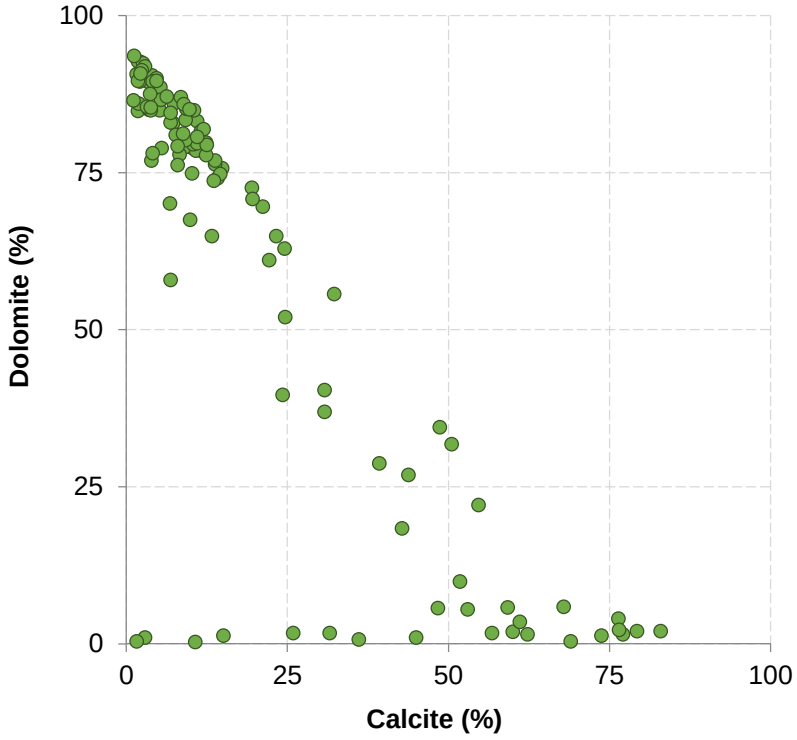

Figure 8. Cross-plot of calcite and dolomite contents in studied whole rock samples (wt %).

Electron microscopy

Electronic images of studied thin sections were collected in backscattered electron (BSE) mode where materials with higher average atomic number (as pyrite, calcite etc.) show up lighter/brighter on electron image. Materials with low atomic number (dolomite, organic carbon) show up on BSE images as darker areas. Using SEM-EDS elemental mapping of thin sections, various elemental distributions were obtained, for the ease of comprehension only chosen elements are presented: Ca, Mg, Si and Al. In most cases Ca in the mapping images represents calcite (calcium carbonate) and dolomite (calcium magnesium carbonate), however, in some cases Ca can also represent calcium phosphate (apatite). The presence of Mg together with Ca is an indicator of dolomite. Si can refer to quartz (silicon dioxide), silicate minerals or if together with Al, K, Fe and Mg, can be considered as a signal from clay-mica minerals (phyllosilicates).

Microstructure in studied dolostones in the central parts of the carbonate horizons is characterized by tightly packed, small (~100 µm), rhombohedral crystals and crystal-aggregates. The (pore)space between dolomite crystallites is typically filled with organic-rich material indicated by high carbon signal, anhedral calcite or silicate minerals (Figure 9a, 10).

In most cases the tightly packed rhombohedral dolomite crystals are rimmed with calcite and interstices between dolomite crystals are filled with silicate minerals and particularly quartz suggesting that calcite (and quartz) occur in this case, respect with dolomite, as later phases.

Images of dolostone thin section made of rock closer to the carbonate – mudstone/chert contacts shows calcite replacing/overgrowing rhombohedral dolomite crystals or occupying most of the pore space between dolomite crystallites (Figure 9b, 11). The interstices between calcite and dolomite aggregates are filled with silicate minerals (mica and talc) and quartz. Occasionally approximately 1 mm long and 0.3 mm wide oval aggregates occur composed of poorly defined dolomite crystals together with calcite, quartz and silicate minerals (mica) (Figure 9c).

Thin section prepared of a carbonate rock next to the carbonate – mudstone/chert contact zone show rhombohedral dolomite crystals overgrown with calcite, and in some cases also zonal calcite-dolomite alteration with massive silica (quartz) aggregate and Mg-rich silicate (talc) filling the pore space (Figure 9d, 12Figure 12).

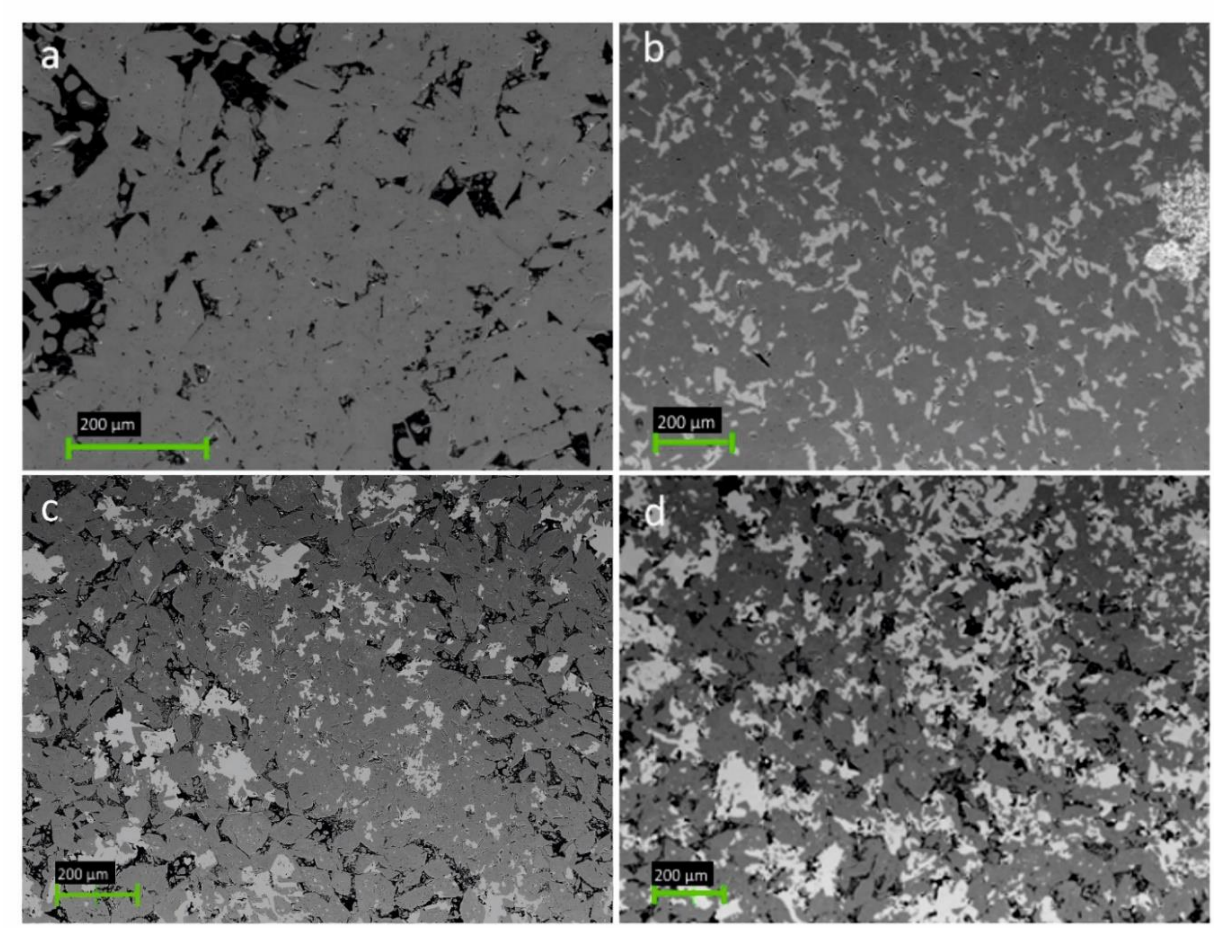

Figure 9. SEM BSE images of (a) massive dolostone composed of tightly packed dolomite crystals, separated by organic-rich material and some other minor minerals; (b) dolostone where calcite and other minerals have filled the space between dolomite crystals; (c) dolostone close to the carbonate-mudstone/chert contact with oval mineral aggregates; (d) dolostone rich in calcite close to the carbonate-mudstone/chert contact

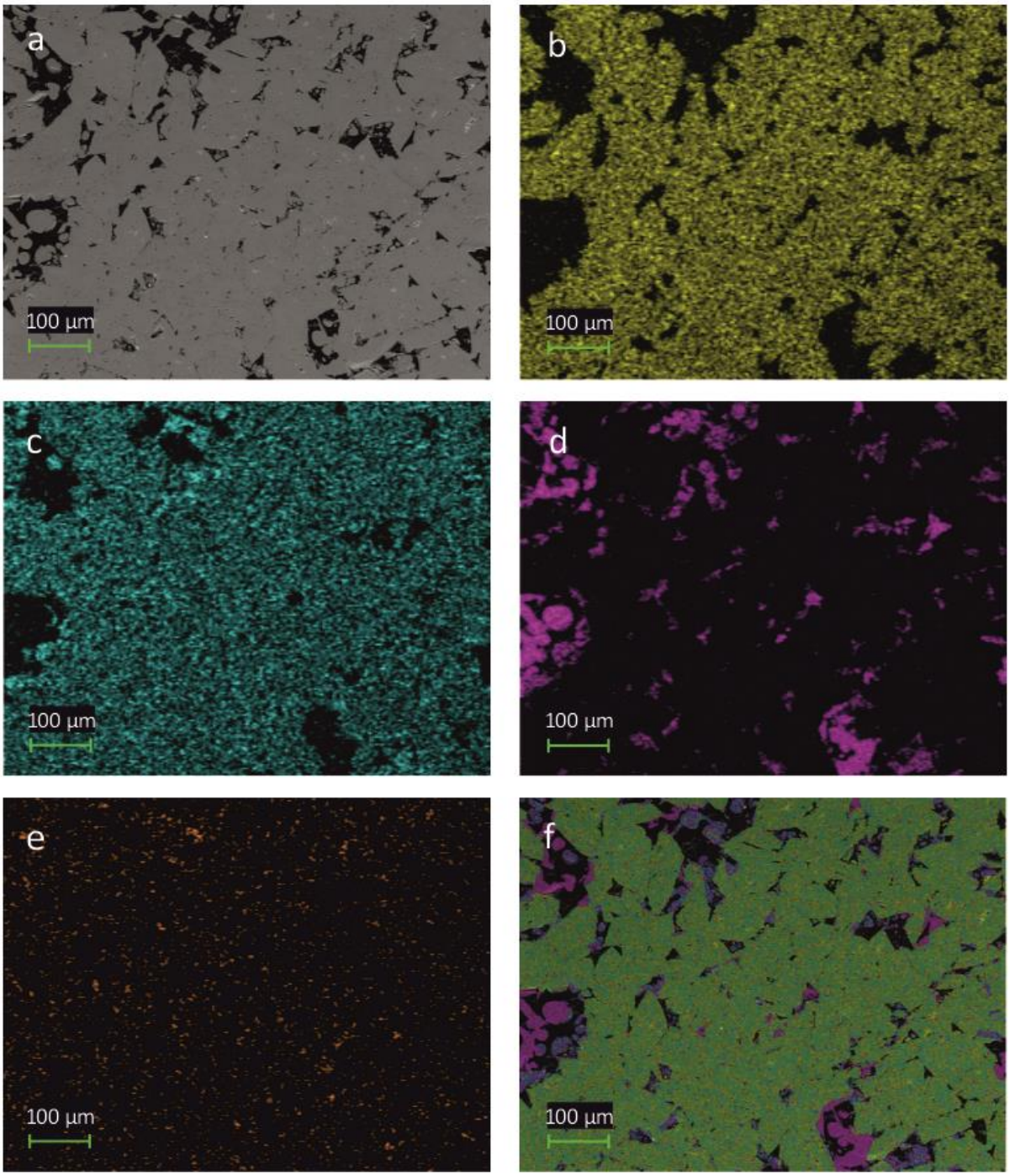

Figure 10. Elemental mapping of thin section from depth 1111.4 m closer to center of the carbonate bed: (a) BSE image; (b) Ca; (c) Mg; (d) Si; (e) Al; (f) overlay image of chosen elements, green represents dolomite, yellow calcite, purple quartz, blue talc and mica.

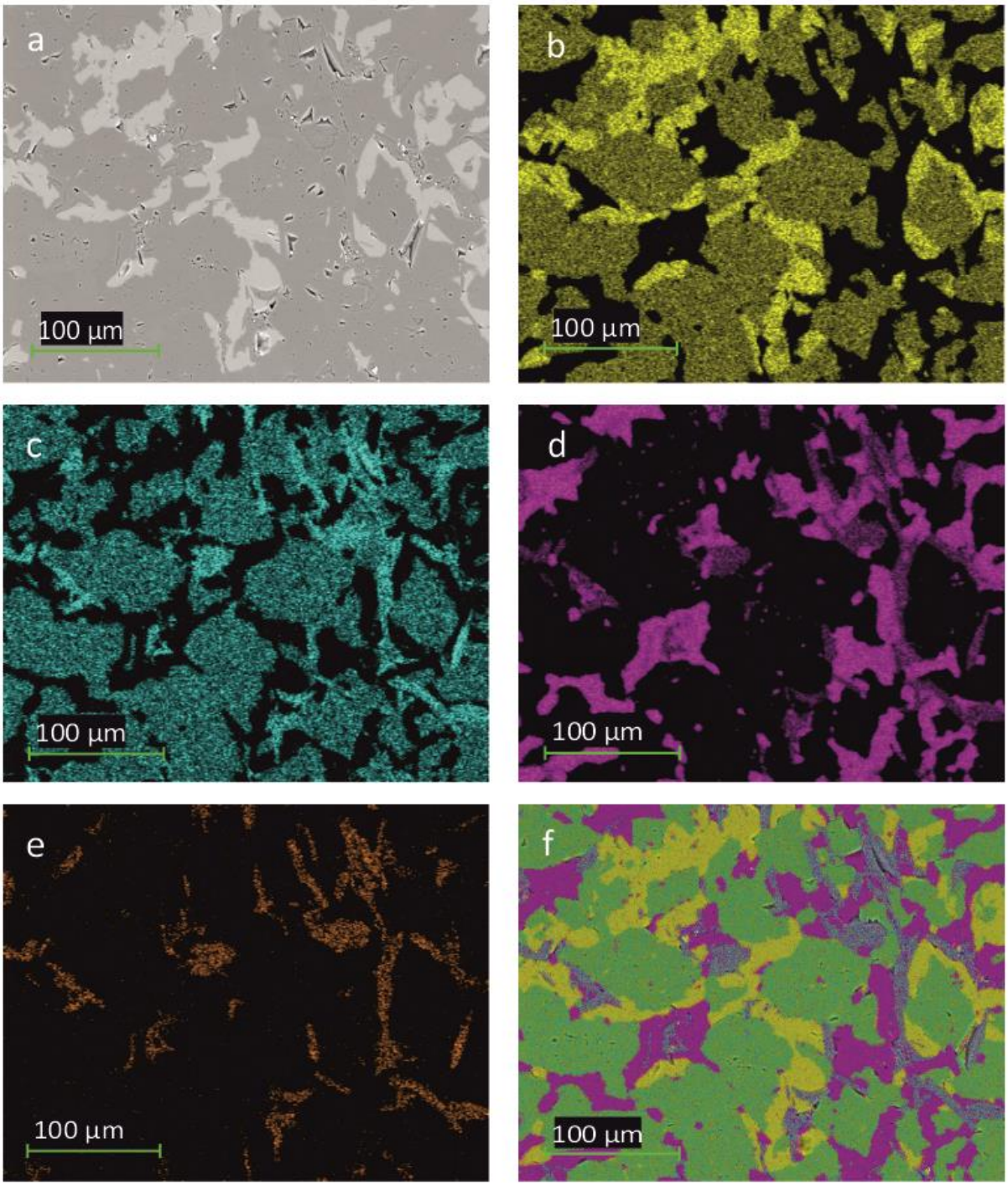

Figure 11. Elemental mapping of thin section from depth 1109.4 m, the central part of the carbonate bed: (a) BSE image; (b) Ca; (c) Mg; (d) Si; (e) Al; (f) overlay image of chosen elements, green represents dolomite, yellow calcite, purple quartz, blue talc and mica.

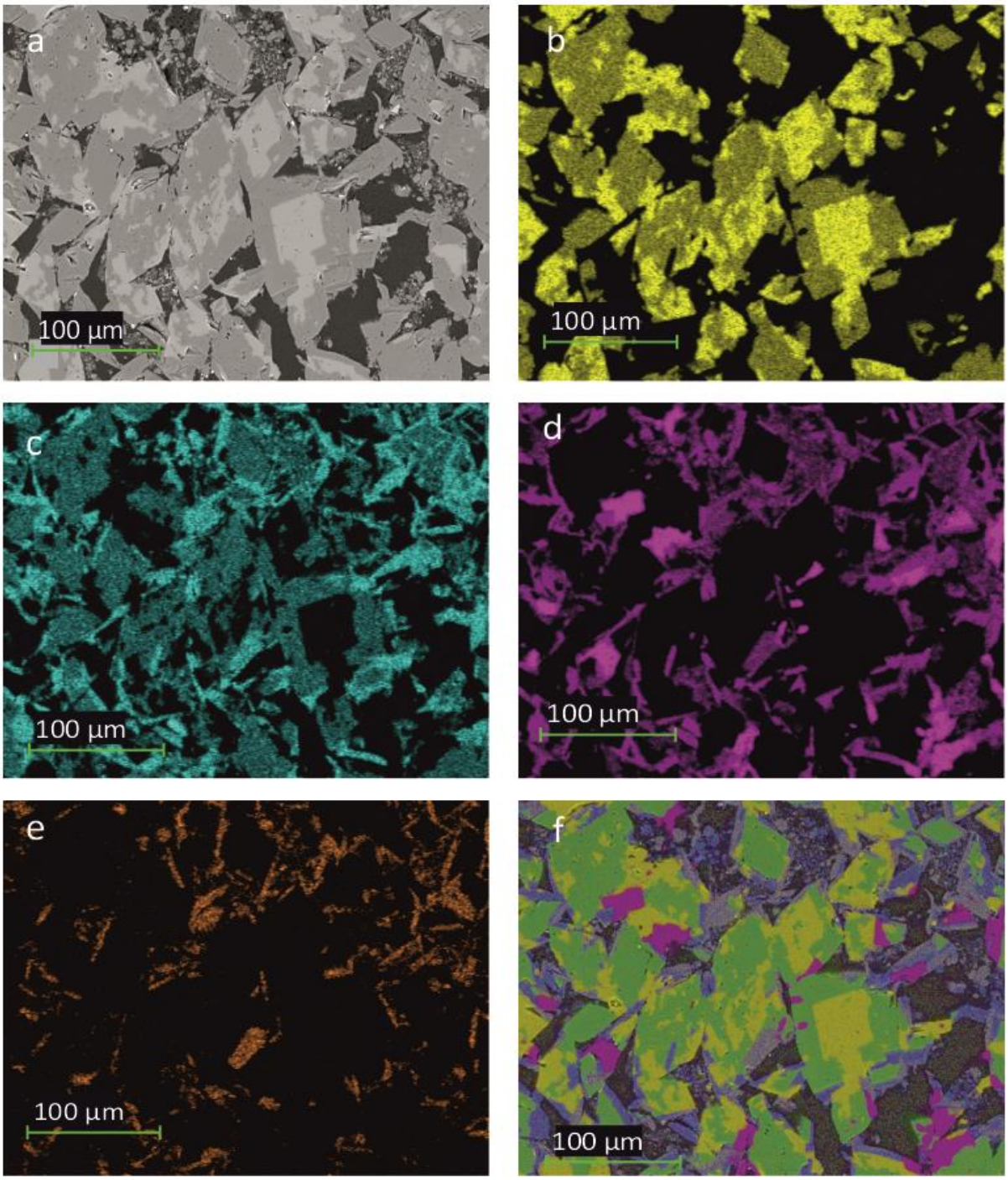

Figure 12. Elemental mapping of thin section from depth 1111.6 m next to carbonate-mudstone/chert contact: (a) BSE image; (b) Ca; (c) Mg; (d) Si; (e) Al; (f) overlay image of chosen elements, green represents dolomite, yellow calcite, purple quartz, blue talc and mica.

Isotope composition

Carbon and oxygen stable isotope composition of studied carbonate rocks is shown in Table 2 in Appendix and Figure 13. $\delta^{13}C_{carb}$ values of carbonate samples show high variation between –17 to 1 ‰. All four carbonate beds display depleted $^{13}C_{carb}$ values close to contacts with mudstone and chert lithologies and considerably higher values of $^{13}C_{carb}$ in the central parts of the beds (Figure 13).

Similarly, the $\delta^{18}O_{carb}$ values show high variability and range from –15 to –5 ‰. The overall trend with respect to position within the carbonate horizon is not as clear as displayed in the case of $\delta^{13}C_{carb}$ variation but the trend of $\delta^{18}O_{carb}$ values from less depleted values in the middle parts of the beds to more depleted values outward to their margins is still traceable (Figure 13).

The $\delta^{13}C_{org}$ values are not as variable as in carbonates, showing values at about –36 ‰ in the lowermost sampled dolostone bed, about –37 ‰ in the layer at the depth 1117 to 1115 m and a slight but steady increase to about –35 ‰ in uppermost studied bed where in short interval the $\delta^{13}C_{org}$ increase to –26 to –24 ‰ at about 1105 m depth (Figure 13). $\delta^{13}C_{org}$ values do not show any systematic variation with respect to carbonate and mudstone/chert contacts though the less depleted $\delta^{13}C_{org}$ values are found in carbonates showing the highest $\delta^{13}C_{carb}$ values (Figure 13)

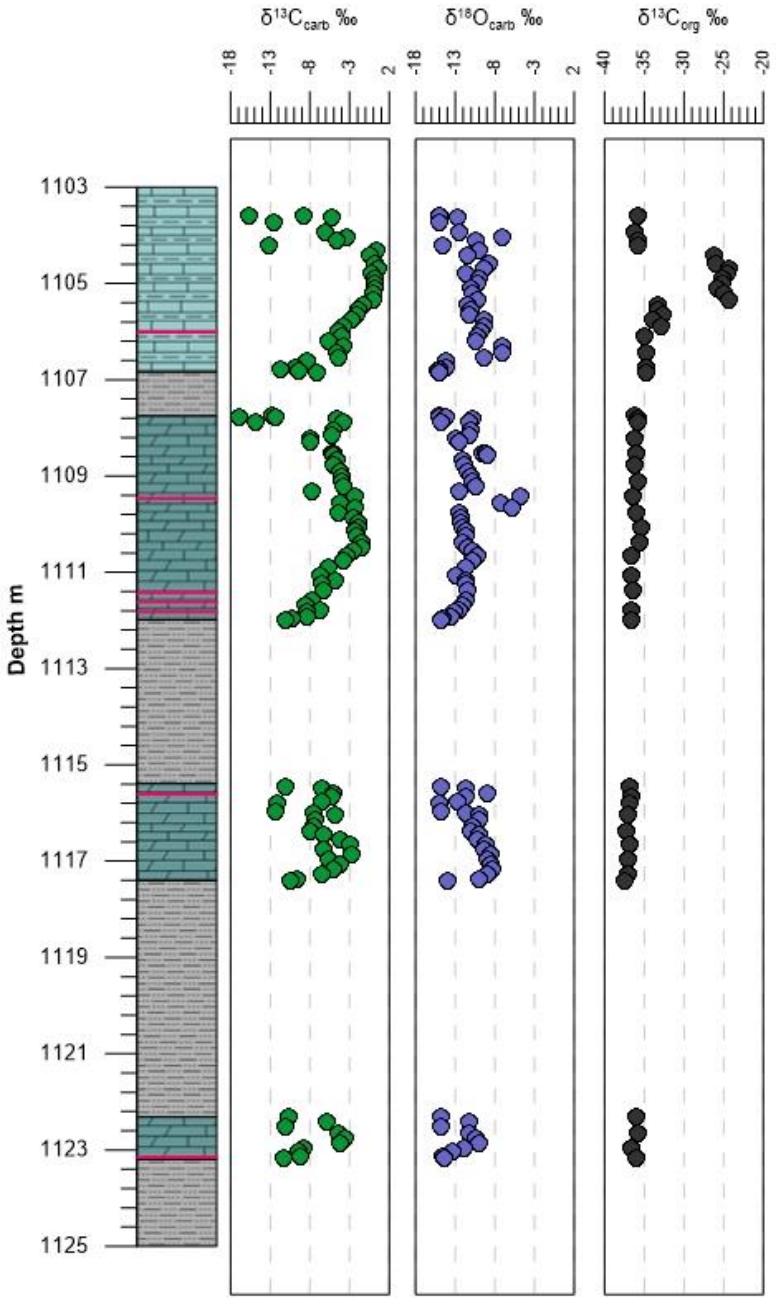

Figure 13. $\delta^{13}C_{carb}$, $\delta^{18}O_{carb}$ and $\delta^{13}C_{org}$ values in samples with respect to depth and lithology.

TOF-SIMS

Lateral distributions and an overlay map of chosen elements measured using TOF-SIMS are shown in Figure 14. The area selected for analysis shows two rhombohedral crystals with surrounding anhedral minerals. The overlay map suggest that the crystallite in the left is composed of Ca, mixed with Mg, and can be described as calcite with dolomite inclusions. The crystal on the right shows signal from Ca^+ and Mg^+ with some Si^+ on the margin, and can be considered as dolomite rimmed with magnesium silicate (talc). Space between two crystals is filled with mineral phases containing Ca, Mg, Si, Na, K and Al, mainly calcite, talc, quartz and clay minerals.

One of the purposes of TOF-SIMS analysis was to obtain lateral distributions of ^{12}C and ^{13}C in different mineral phases, during the analysis it became clear that even with the high mass resolution the content of $^{13}C^-$ is so low that intensive signal from $^{12}C^-$ together with H was strongly interfering the signal from $^{13}C^-$. Hence in current sample observation of lateral distribution of different C isotopes was unattainable with this method.

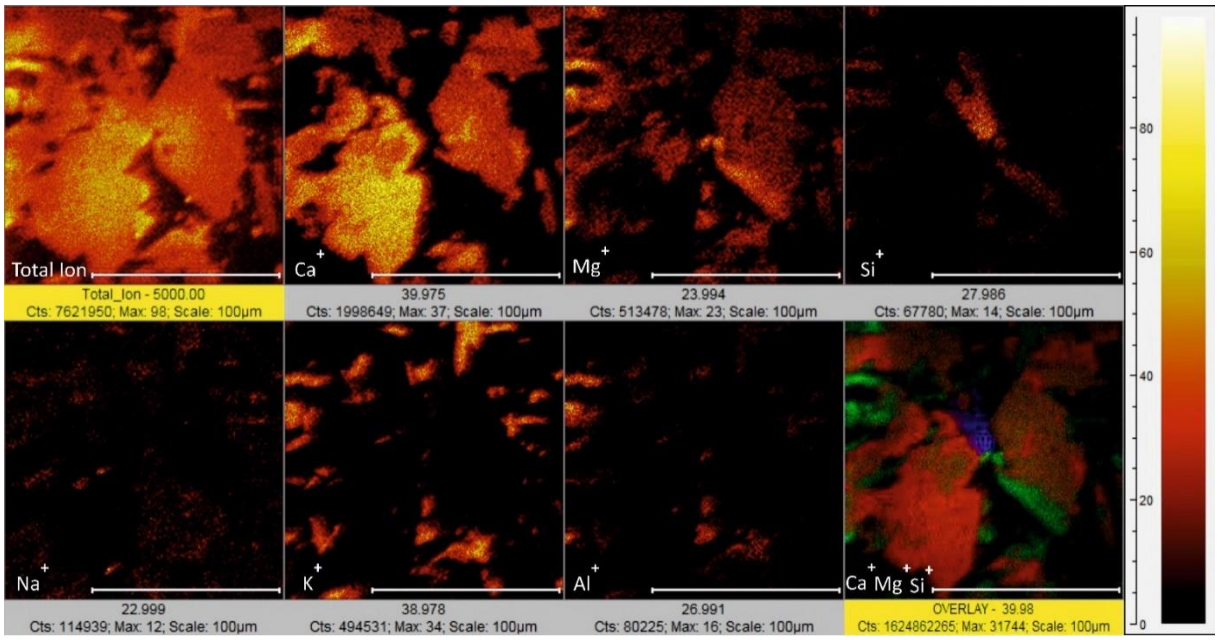

Figure 14. Mapping images of TOF-SIMS showing the lateral distributions of Ca^+, Mg^+, Si^+, Na^+, K^+, Al^+ and overlay map of Ca^+ (red), Mg^+(green) and Si^+ (blue) of chosen area.

Discussion

Carbonate rocks are typically considered retaining syndepositional $\delta^{13}C_{carb}$ values under diagenetic or even at metamorphic recrystallization (Schidlowski, 2001) whereas the oxygen isotopic composition of the carbonate minerals is typically reset during recrystallization (Banner and Hanson, 1990). However, in the presence of silicate mineral phases also the isotopic composition of carbon becomes re-equilibrated under metamorphic conditions with metamorphic fluids and/or decarbonation reactions (Valley, 1986). Also, both $\delta^{13}C_{carb}$ and $\delta^{18}O_{carb}$ values are significantly altered at much lower temperatures/pressure regimes compared with metamorphic by meteoric diagenesis and diagenetic/hydrothermal dolomitization (Knauth and Kennedy, 2009). Even the classical covariant $\delta^{13}C_{carb}$ and $\delta^{18}O_{carb}$ record that has been interpreted as evidence that both the carbonate and organic matter were originally produced in the surface waters of the ocean, and that they have retained their original $\delta^{13}C_{carb}$ composition (e.g. Knoll *et al.,* 1986; Swanson-Hysell *et al.,* 2010) was recently shown to be mimicked by meteoric alteration (Oehlert and Swart, 2014). As the result of these diagenetic-metamorphic processes the isotopic composition of carbonate phases deviates from primary seawater equilibrated values and is controlled by the composition of the original sediment and fluid, fluid/rock ratio during alteration, porosity, isotope fractionation factors, distribution coefficients and open-system versus closed-system behavior (Banner and Hanson, 1990).

Changes in the carbon isotopic composition of marine carbonates, especially globally recognized isotopic excursions/events recorded in marine $\delta^{13}C_{carb}$ composition are interpreted to reflect global changes in the carbon cycle, and used to model the ancient environments (e.g. Kaufman and Knoll, 1995; Holland, 2004). It is therefore of utmost importance that the nature of isotopic values of marine carbonate sequences, original syndepositional and/or altered, is established.

Moreover, earlier studies have shown that carbonate $\delta^{13}C$ values in the Zaonega Formation can be as low as −25 ‰ and as high as 10 ‰ (Melezhik *et al.*, 1999; Krupenik *et al.*, 2011; Kump *et al.*, 2011). Such depleted $\delta^{13}C_{carb}$ values of carbonate have been interpreted as resulting from methanotrophy and/or due to depleted isotopic composition of dissolved inorganic carbon linked to atmospheric oxidation of methane (Yudovich *et al.*, 1991). Alternatively, Krupenik and others (2011) have suggested that carbonates of Zaonega Formation have been diagenetically recrystallized and the depleted $\delta^{13}C_{carb}$ values reflect incorporation of carbon derived from oxidized organic matter.

Indeed, such fluctuating trends, particularly over a short distances in the rock record like in studied core, are indicative of post-depositional resetting of C and O isotope systems (e.g. Jacobsen and Kaufman, 1999). The rock sequence of Zaonega Formation exposed in Onega basin has underwent greenschist facies metamorphism and the whole section has been influenced by intensive hydrothermalism (Melezhik *et al.,* 1999). Therefore, it is plausible to expect that the mineral, chemical as well as isotopic composition of these deposits has been altered at least to some extent.

Recently, Črne and others (2014) studied eight carbonate beds (varying in thickness from 0.3 to 0.9 m) of Zaonega Formation exposed in FAR DEEP drillcore 12A and 13A showing variation of $\delta^{13}C_{carb}$ values as large as 17 ‰. Their studies showed, using sequential dissolution technique (Al-Aasm *et al.,* 1990), that the carbon isotopic signal carried by calcite was significantly depleted in ^{13}C relative to dolomite occurring in the same beds. They interpreted the ^{13}C-depleted calcite representing a late-diagenetic to metamorphic phase that incorporated carbon derived from diagenetic-catagenetic alteration of organic matter and possibly volcanic CO_2, whereas the observed mineral association of calcite ± talc ± phlogopite ± actinolite suggests metamorphic reaction of dolomite with quartz (or K-feldspar) that caused degassing of ^{13}C-enriched CO_2 and crystallization of ^{13}C depleted calcite (Črne *et al.*, 2014).

Similar to earlier studies, the Zaonega Formation carbonate rocks exposed in OPH drillcore which are studied in this thesis show large variation of $\delta^{13}C_{carb}$ and $\delta^{18}O_{carb}$ values fluctuating between –17 to 1 ‰ and –15 to –5 ‰, respectively. The most depleted $\delta^{13}C_{carb}$ values of sampled carbonate rocks are found symmetrically at the upper and lower boundaries of the carbonate beds (Figure 13) and the covariation with the mineral composition suggest that the most depleted $^{13}C_{carb}$ values can be associated with calcite, as far as all carbonate beds show the most depleted $^{13}C_{carb}$ values and highest calcite content close to contacts with other rock layers and the less depleted $^{13}C_{carb}$ values and the higher dolomite content is found in the central parts of the beds (Figure 7).

Covariation of the calcite and dolomite content according to XRD analyses and the carbonate isotope composition of the same minidrilled powders clearly indicates a mixing between (at least) two end-members: calcite with $\delta^{13}C_{carb}$ isotopic composition varying between –17 to –7 ‰ in samples with relative calcite content >80 %wt of carbonate minerals; (Figure 15, 16b) and dolomite with $\delta^{13}C_{carb}$ values ranging from –10 to 1 ‰ in samples with relative dolomite content >80 %wt (Figure 16a). It is even more interesting that $\delta^{18}O_{carb}$ versus mineral composition show that calcite end-member (samples with relative calcite content >80 %wt) shows a narrowly

defined isotopic composition at –15.1 to –14.5 ‰ while dolomite $\delta^{18}O_{carb}$ values vary between –12.5 to – 4.5 ‰ in samples with relative dolomite >80 %wt (Figure 17).

Črne and others (2014) have suggested, based on $\delta^{13}C_{carb}$ values variation respect with calcite and dolomite, that dolomite is primary sedimentary carbonate phase with higher $\delta^{13}C_{carb}$ values and calcite was regarded as a later phase formed during burial and metamorphism together with possible hydrothermal alteration and metamorphic carbonate-silicate reactions. Results of this thesis concur with earlier findings and suggest that (i) the oxygen isotopic composition of calcite was completely reset during recrystallization and its value represents the properties of the diagenetic/hydrothermal/metamorphic fluid, and (ii) the carbon isotopic composition of calcite and possibly dolomite was partially reset or the carbon was derived from different sources with different isotopic signal during the recrystallization.

Črne and others (2014) interpreted calcite crystallization Zaonega Formation dolostones at near to contacts with silicate rock as mainly driven by calcite ± talc ± phlogopite ±actinolite paragenesis (See Eq. 1). This mineral association commonly develops in dolomitic rocks which have been subjected to low-temperature, greenschist-facies metamorphic alteration and imply to dolomite reaction with silicates to produce calcite, talc and other silicate minerals. During calcitization the Mg released from dolomite is bound into talc, phlogopite or actinolite. This process is accompanied by degassing of both ^{13}C and ^{18}O enriched CO_2 thus leaving behind carbonates which have been depleted in ^{13}C and ^{18}O (Valley, 1986; Črne *et al.*, 2014).

$$6[Ca, Mg(CO_3)_2] + 8SiO_2 + 2H_2O \rightarrow Mg_6[Si_8O_{20}](OH)_4 + 6CaCO_3 + 6CO_2 \quad (1)$$

However, this process would predict, even in the case of open-system devolatization, isotopic depletion with respect ^{18}O and ^{13}C in the order of few per mil maximum (Valley, 1986). The magnitude of $\delta^{13}C_{carb}$ depletion of calcite relative to dolomite in Zaonega Formation carbonates in studied beds in OPH core is up to 17 ‰ and up to 10 ‰ for $\delta^{18}O_{carb}$ values. Such depletion cannot be explained by calcite ± talc ± phlogopite ±actinolite paragenesis (Eq. 1) alone. Moreover, the mineralogical data and scanning electron microscopy observation show that calcite precipitation at carbonate bed contacts is always accompanied with (replacive) precipitation of silica in the pore space of the crystalline dolostone that does not agree with the metamorphic reaction (Eq.1) of the dedolomitization. Metamorphic recrystallization is possibly

present as evidenced by calcite ± talc ± phlogopite ±actinolite paragenesis, but is particularly developed at the lower contacts of the carbonate beds whereas dolomite-calcite replacements shows a symmetrical distribution at both contacts (see Figure 7).

This suggest that the mineral and isotopic composition of the carbonate beds in Zaonega Formation was mainly influenced by enhanced input of ^{13}C and ^{18}O depleted fluid from an external source. Such fluid could have been supplied by contemporaneous magmatic activity and hydrocarbon generation taking place during the deposition of Zaonega rocks. Sedimentary sequence of the Zaonega Formation alternates with numerous syndepositional tuff beds and lavas, and contains sills intersecting or interlayering sedimentary beds indicating high volcanic activity during the deposition (Črne *et al.*, 2013a). Peperite contacts of some gabbro sills within hemipelagic mudstones indicate that the intrusion of magmatic bodies occurred when the sediments were still wet and unconsolidated. It is possible that these intrusions triggered hydrothermal circulation and initiated hydrocarbon formation and migration (Melezhik *et al*., 1999; Črne *et al.,* 2013a; b). Hydrothermal fluids carrying silica, CO_2 and possibly CH_4 were ^{13}C depleted and resulted in hydrothermal fluid-rock interaction at low metamorphic temperatures (Strauss *et al.,* 2013).

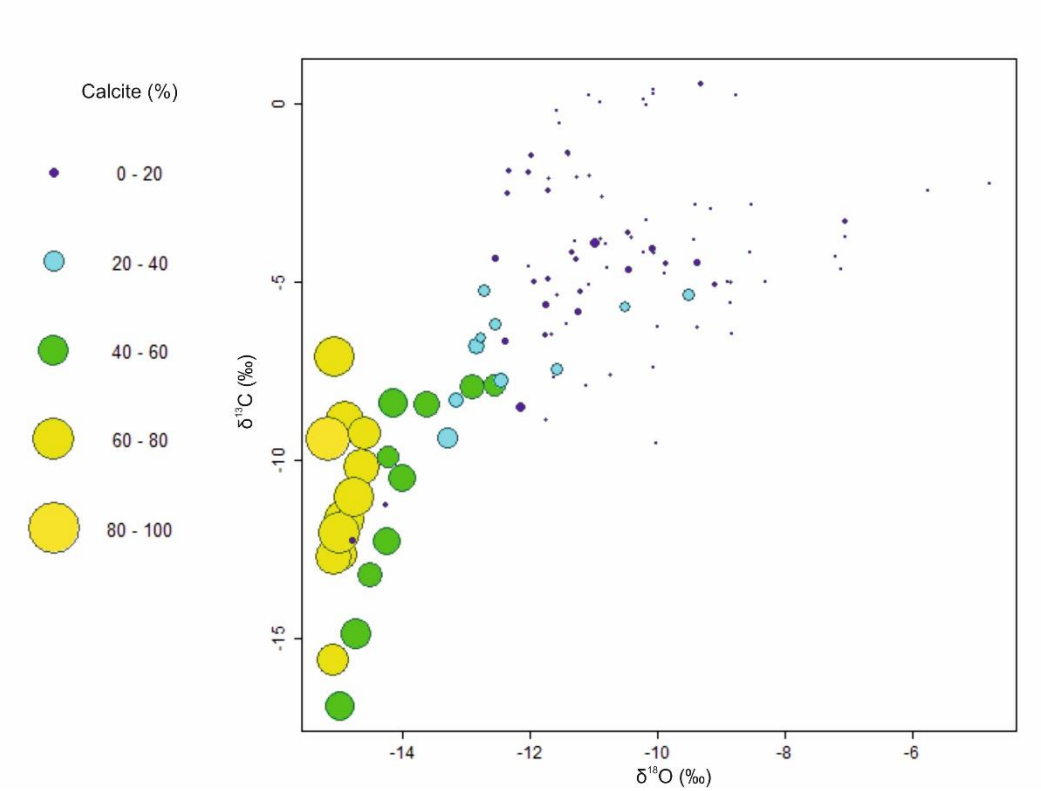

Figure 15. Cross plot of $\delta^{18}O_{carb}$ and $\delta^{13}C_{carb}$ values, circles represent calcite content in whole rock.

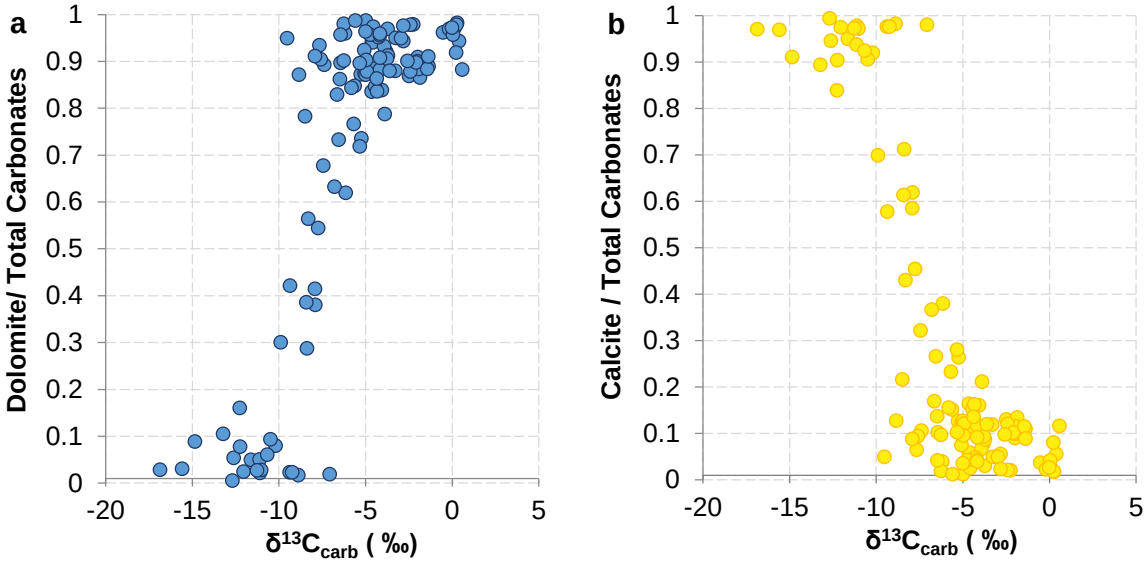

Figure 16. Cross-plotted values of (a) $\delta^{13}C_{carb}$ and relative dolomite content in total carbonates, and (b) $\delta^{13}C_{carb}$ and relative calcite content in total carbonates.

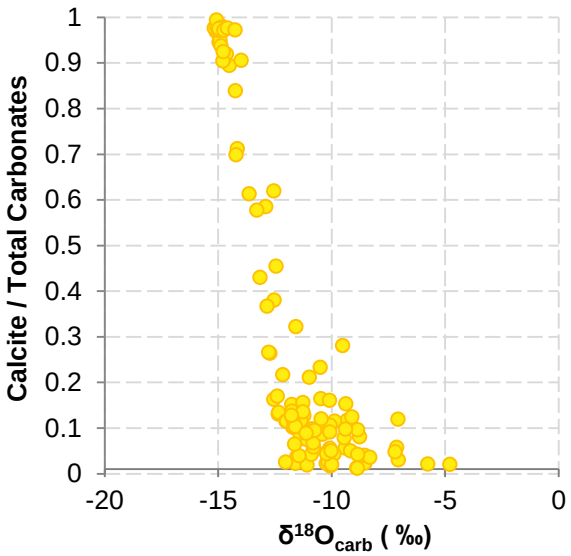

Figure 17. Cross plotted values of $\delta^{18}O_{carb}$ and relative calcite content in total carbonates.

The carbon isotopic composition of carbonate minerals is mainly controlled by the carbon isotopic composition of dissolved inorganic carbon (DIC), given that the fractionation between DIC and the calcium carbonate precipitating in the system is small, and kinetic effects are negligible (Romanek *et al.*, 1992; Frisia *et al.*, 2011). Sources of ^{13}C depleted dissolved inorganic carbon in Zaonega Formation may have been: (i) volcanic CO_2 with $\delta^{13}C$ value of around –5 ‰, (ii) products of decomposition/oxidation of organic material with $\delta^{13}C$ between –25 and –42 ‰ and (iii) products of catagenesis of organic material (organic acids, biogenic and thermogenic methane) with $\delta^{13}C$ ranging from –20 to –50 ‰ (Qu *et al.*, 2012). However, though it is possible that volcanic CO_2 contributed to these hydrothermal fluids then it is evident that it would not have facilitated formation of calcite with $\delta^{13}C$ values well below 0 ‰. The most probable source of ^{13}C-depleted CO_2 and the dissolved bicarbonate used up for calcite precipitation was organic matter with $\delta^{13}C$ values between –25 and –42 ‰, which went through thermal and bacterial oxidation involving reduction of sulphates and/or Fe- Mn-oxyhydroxides. Another possible source, the oxidation of CH_4 e.g. through anaerobic methane oxidation (AOM), is unlikely because none of the obtained $\delta^{13}C$ values in calcite rich carbonates are lower than –17 ‰. AOM derived carbonates using up dissolved inorganic carbon from oxidation of methane show at modern and ancient methane seeps $\delta^{13}C$ values well bellow –20 ‰ (e.g. Campbell, 2006). However, the contribution of methane as source for depleted carbon cannot be completely ruled out because it should be taken into consideration that both biogenic and thermogenic CH_4 were likely available at the site and the thermogenic methane is typically

characterized by higher $\delta^{13}C$ values over –50 ‰ (up to −22±3 ‰ in pyrogenic methane, Whiticar, 1999; Sapart *et al.*, 2012).

Moreover, if we assume that the main source for the different DIC species in the fluid circulating in Zaonega rocks was CO_2 produced by decomposition of organic matter with a $\delta^{13}C$ values of –35 to –25 ‰ as suggested from $\delta^{13}C_{org}$ values in OPH carbonates then, considering fractionation between CO_2 – bicarbonate – calcite (e.g. Breecker *et al.*, 2012), the secondary calcite would display, without a host-rock contribution, the carbon isotopic ratios of –19 to –11 ‰. This agrees well with the observed values of isotopic composition of carbon in the most calcite–rich samples in studied OPH section.

Classically, the cross-plot of $\delta^{13}C$ and $\delta^{18}O$ is used to assess the effect of diagenesis, which is usually marked by depletion of ^{18}O (Burdett *et al.*, 1990). However it is also possible that the $\delta^{13}C$ vs $\delta^{18}O$ correlation represents post-depositional modification of both carbon and oxygen isotopes, instead. In that case $\delta^{13}C$ and $\delta^{18}O$ values are unrepresentative about the global marine inorganic carbon reservoir. For example, Knauth and Kennedy (2009) and Derry (2010) proposed that $\delta^{13}C$ and $\delta^{18}O$ correlations may express early diagenesis in the presence of ^{13}C-poor meteoric waters or several generations of fluid-rock interactions at high temperatures.

Measured $\delta^{13}C_{carb}$ and $\delta^{18}O_{carb}$ values (Figure 18) show a complex non-linear co-variation which possibly reflects different level of alteration/resetting of isotopic composition. Jacobsen and Kaufman (1999) have shown, using mass-balance modelling, that partial resetting of the oxygen isotopic system in carbonates due to fluid-rock interaction would result in an $\delta^{13}C_{carb}$ and $\delta^{18}O_{carb}$ trend paralleling the oxygen axis. However, during the complete resetting carbon and oxygen isotope composition would result in a trend where $\delta^{18}O_{carb}$ and $\delta^{13}C_{carb}$ eventually reach values which differ from fluid $\delta^{18}O_{carb}$ and $\delta^{13}C_{carb}$ values only by the water-rock fractionation factor (Banner and Hanson, 1990; Jacobsen and Kaufman, 1999).

Interestingly, assuming that the variation of isotopic values measured in OPH carbonates reflect the different progress in the recrystallization, then the cross-plotted values of $\delta^{18}O_{carb}$ and $\delta^{13}C_{carb}$ (Figure 18) cannot be explained by a single alteration episode model. The isotopic values show, in this sense, two or even three rock-water alteration trends suggesting that, theoretically, at least three different fluid-rock interaction episodes occurred after deposition of this interval resetting completely or partially the original isotopic composition.

To assess the rock-water interaction in terms of isotopic composition of host rock and secondary calcite in Zaonega Formation carbonate beds numerical models for closed (Eq 2) and open

system alteration after Jacobsen and Kaufman (1999) (Eq 3, Figure 19) for finding possible parameters for different fluid-rock interaction episodes, were made.

$$\delta_i^r(\eta) = \frac{\left(\frac{C_i^{ro}}{C_i^{wo}}\right)\delta_i^{r0} + \eta\,(\delta_i^{wo} + \Delta_i)}{\eta + \left(\frac{C_i^{ro}}{C_i^{wo}}\right)} \tag{2}$$

$$\delta_i^r(\eta) = \frac{\left(\frac{C_i^{ro}}{C_i^{wo}}\right)\delta_i^{r0} + D_i\left[exp\left(\frac{\eta}{D_i}\right) - 1\right][\Delta_i + \delta_i^{wo}]}{\left\{\left(\frac{C_i^{ro}}{C_i^{wo}}\right) + D_i\left[exp\left(\frac{\eta}{D_i}\right) - 1\right]\right\}} \tag{3}$$

where δ_i^r is the final isotopic composition η the weight ratio of fluid to rock, C_i^{ro} and C_i^{wo} initial concentration of element *i* in the rock and in the fluid respectively, D_i is effective rock-fluid distribution coefficient, Δ_i is fluid-rock exchange fractionation factor for element *i* and δ_i^{wo} is the initial isotopic composition of the fluid.

The temperature of the system is included in Δ_i value, where the relationship between Δ_i and temperature (T) in Kelvins is expressed with Equation 4 (Friedman and O'Neil, 1977).

$$1000 ln\Delta_i = 2.78 \times 10^6 \times T^{-2} - 2.89 \tag{4}$$

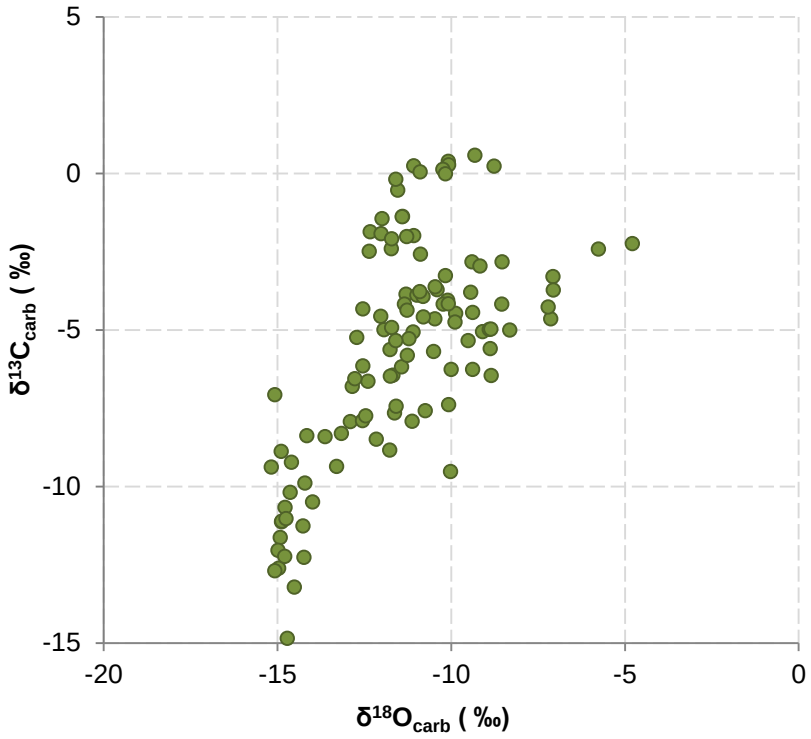

Figure 18. Cross-plotted values of $\delta^{13}C_{carb}$ and $\delta^{18}O_{carb}$ in all samples.

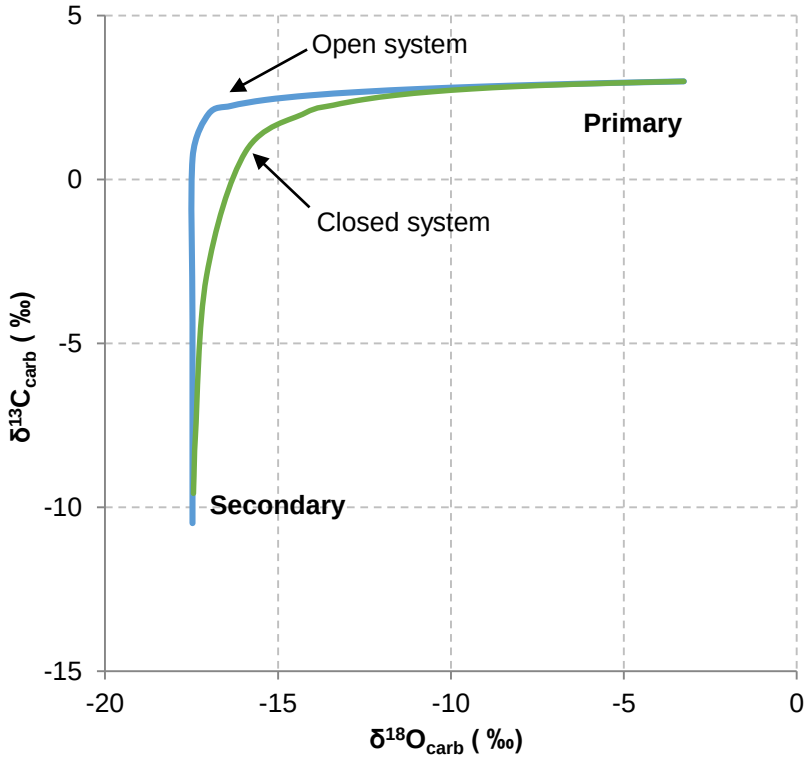

Figure 19. Expected evolution during fluid-rock interaction of $\delta^{18}O_{carb}$ and $\delta^{13}C_{carb}$ for both open and closed systems. Used values in the model are: limestone initial composition: $\delta^{18}O$= –3, $\delta^{13}C$=3, Initial fluid composition: $\delta^{18}O^{w0}$=–27, $\delta^{13}C^{w0}$ =–10, C_C =0.5, D_O=0.54, D_C=24, T=200 °C.

In order to make the model some physical parameters were chosen to describe environment where the interaction occurred. The upper temperature limit was chosen at 200 °C which is the higher limit of catagenesis for organic material, although Melezhik and others (1999) have suggested that some generations of carbonates may have formed under greenschist facies (300-450 °C) conditions. The fluid $\delta^{18}O$ value was limited between –25 to –20 ‰ VPDB (5 to 10 ‰ SMOW), which is the composition of primary magmatic waters (Sheppard, 1986) since the formation of Zaonega succession was accompanied by contemporaneous magmatic activity. The same range of fluid composition is characteristic for most of the deep hydrothermal waters (Sheppard, 1986).

Open system modeling was mainly used, since the weight ratio of fluid to rock for altered carbonate rock stays in the range of 1 to 10 the closed system model is not realistic for those rocks (Jacobsen and Kaufman 1999). Moreover, the minimum values of $\delta^{18}O$ and $\delta^{13}C$ in Zaonega carbonate rocks are –15 and –17 ‰ respectively, such degree of depletion in ^{13}C cannot be explained with a closed system, which means that the fluid interacting with the rock had an external source of isotopically depleted carbon.

Modeling results suggest that calcite precipitation resulted from an interaction involving a ^{18}O and ^{13}C depleted fluid with relative carbon concentration 0.5, $\delta^{18}O$ and $\delta^{13}C$ (assuming bicarbonate as dominant species) values –24.5 and –25 ‰, respectively, interacting with precursor rock (dolomite) characterized by $\delta^{18}O$ and $\delta^{13}C$ values of –10 and –7.5 ‰ (purple in Figure 20). A reasonable fit with observed values was obtained assuming an open system interaction at temperature of 200 °C. It is particularly interesting that this precursor phase could have formed through an interaction involving two different systems. First, a fluid which had temperature of 170 °C, relative carbon concentration 0.2, $\delta^{18}O$ value of –23 ‰ and $\delta^{13}C$ value of –20 ‰ reacted with a precursor carbonate rock with $\delta^{18}O_{carb}$ and $\delta^{13}C_{carb}$ values of –8.5 and 0.5 ‰ respectively (green in Figure 20). Secondly, carbonate rock characterized by $\delta^{18}O_{carb}$ and $\delta^{13}C_{carb}$ values of –4.5 and –2 ‰ respectively interacted with fluid at 180 °C, with relative carbon concentration in of 0.5, $\delta^{18}O$ value of –22 ‰, $\delta^{13}C$ value of –22 ‰ (blue in Figure 20). Both systems are considered to be open systems.

However, we must consider that the measured isotopic values to not represent discrete phases but physical mixtures of different carbonate minerals and the petrographic relationships between calcite and dolomite suggest a multistage crystallisation sequence representing first generation of dolomite as a primary phase, secondary calcite possibly formed by fluid–rock

interaction, and possibly followed by a secondary dolomite which nature is unclear (see Figures 10, 11, 12). Understanding on the nature of this late dolomite, if present, awaits for *in situ* isotopic and trace element characterization. However, the hypothesis that there has been at least three different fluid-rock interaction episodes is also supported by cross-plots of $\delta^{18}O_{carb}$ and $\delta^{13}C_{carb}$ relative to dolomite and/or calcite content which seemingly reveal mixing between three end-members (Figure 21, 22). Spread of the isotopic composition of dolomite-rich samples between –12 and –5 ‰ for $\delta^{18}O_{carb}$ and –10 and 1 ‰ for $\delta^{13}C_{carb}$ might reveal not only variation of the composition and conditions in the sedimentary basin and during early diagenesis, but ratio between of at least two (if not more) nonconcurrent dolomite generations, which have formed under different chemical and diagenetic/metamorphic/hydrothermal conditions.

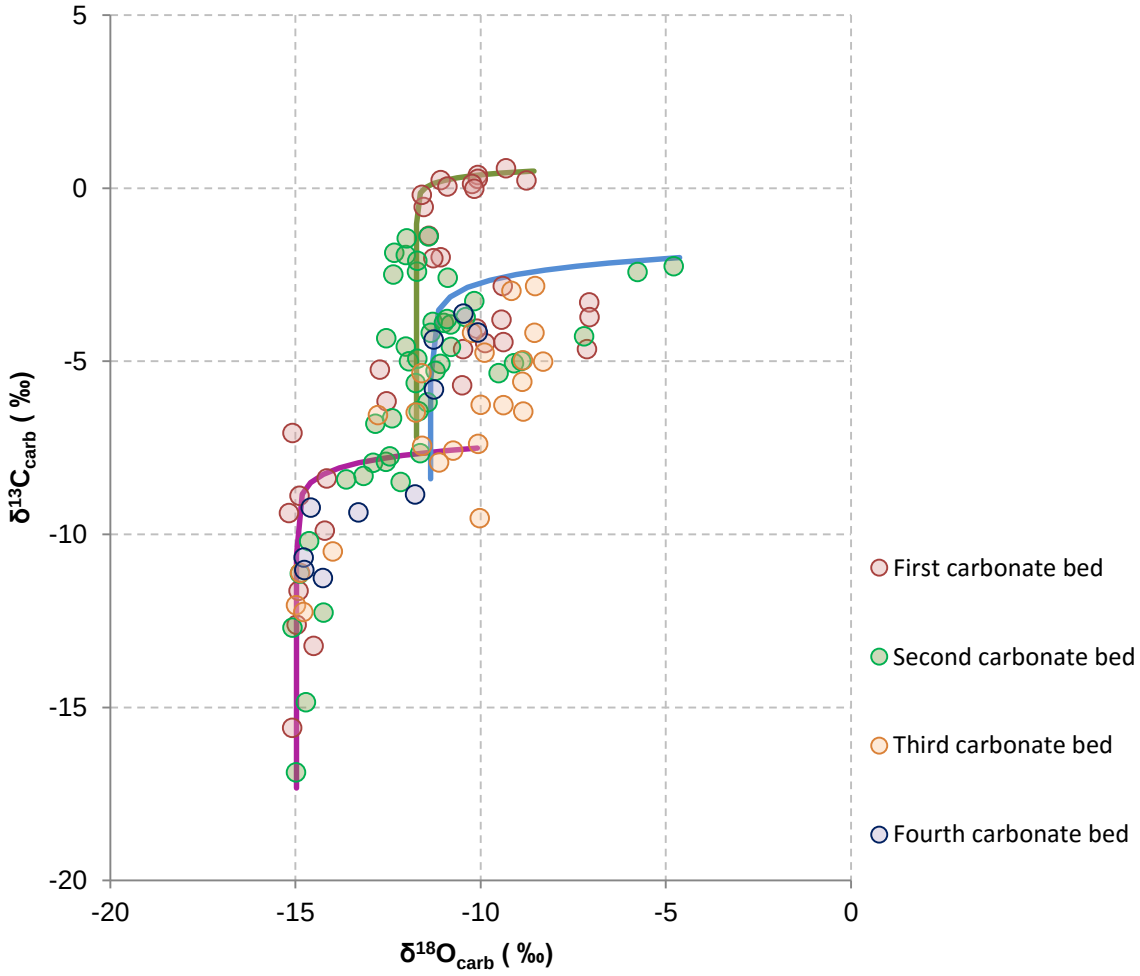

Figure 20. Cross-plotted values of $\delta^{18}O_{carb}$ and $\delta^{13}C_{carb}$ with three possible alteration trendlines in open system after Jacobsen and Kaufman (1999) model.

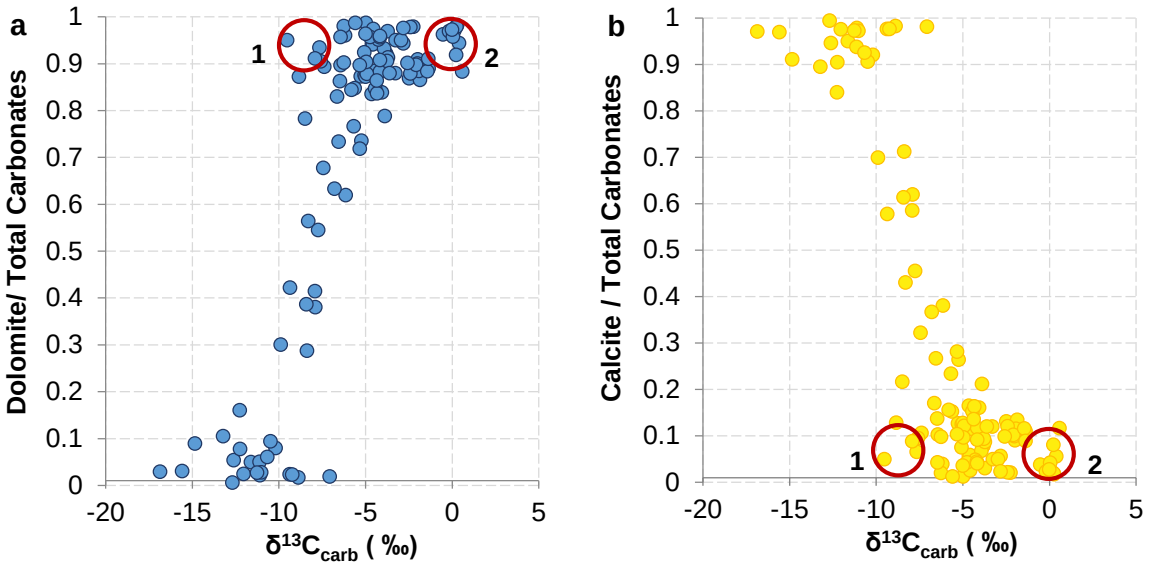

Figure 21. Cross-plotted values of (a) $\delta^{13}C_{carb}$ and relative dolomite content in total carbonates, and (b) $\delta^{13}C_{carb}$ and relative calcite content in total carbonates, with two dolomite end members.

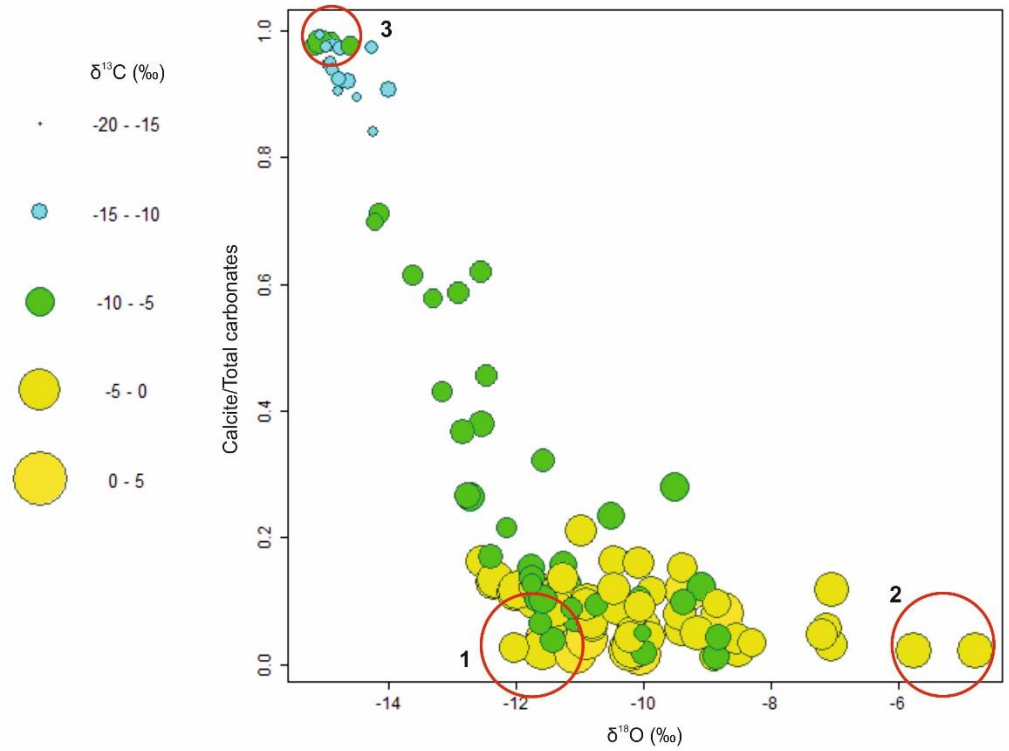

Figure 22. Cross plotted values of $\delta^{18}O_{carb}$ and relative calcite content in total carbonates with two dolomite and one calcite end-members, circles represent $\delta^{13}C_{carb}$ values.

The alteration scenario in Zaonega carbonates is evidently complicated but in general it can be described as multi-staged post-depositional fluid-rock interaction process (Figure 23), where ^{18}O and ^{13}C depleted fluid changes through the interaction the isotope composition of primary carbonate rock (dolostone) towards more depleted values. Moreover, the mineralogy of original carbonate rock (step A in Figure 23) was changed via interaction with SiO_2-rich fluid, resulting in precipitation of calcite and silicate minerals and removal of ^{13}C-enriched CO_2. The changes in the mineralogy, oxygen- and carbon isotopic signature may have been contemporaneous. Such fluid events may have occurred in three episodes (step B in Figure 23) and they were introduced via thin mudstone layers interbedded between dolostones which resulted in generation of new minerals (calcite, talc and mica), chert (Üpraus, 2014) and ^{18}O and ^{13}C-poor carbonates on the margins of the beds or even throughout the carbonate horizon (step C in Figure 23).

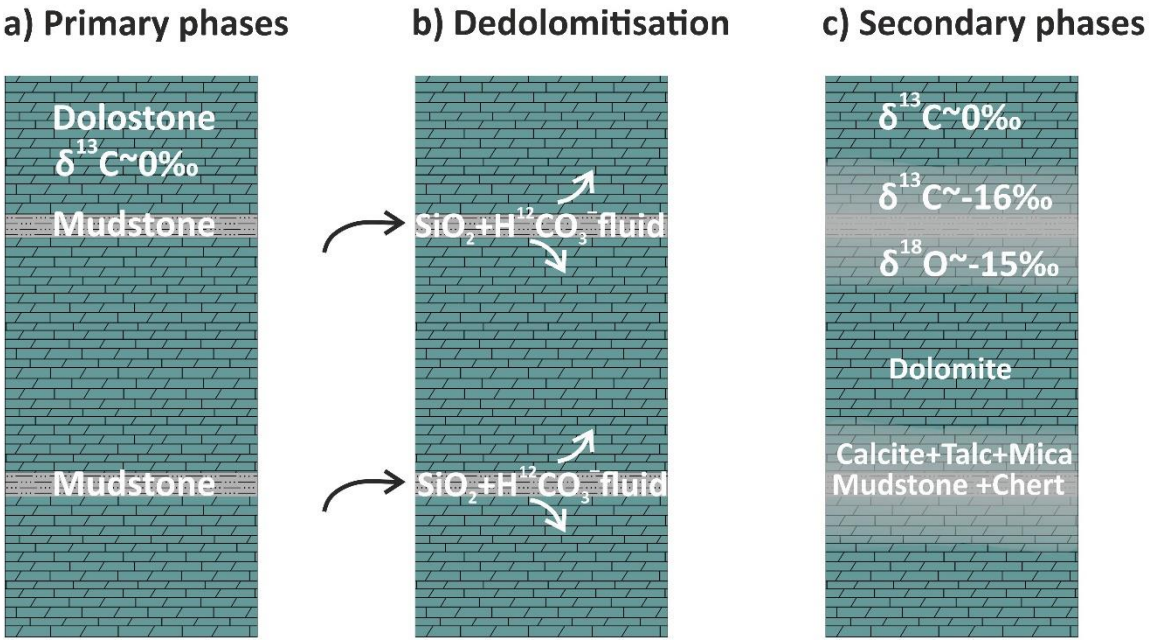

Figure 23. Schematic model of fluidal secondary process altering the mineralogy and isotope composition**.**

Implications to the original isotopic composition of Zaonega dolostones

Carbonate rocks in studied interval are considerably affected by post-depositional alteration and $\delta^{13}C_{carb}$ and $\delta^{18}O_{carb}$ cannot be used without careful screening as the proxy for primary depositional signature. After examining the data I could consider few samples, taken from the

centers of dolostone horizons and having the dolomite content >80 %wt (and possibly $\delta^{18}O_{carb}$ about –10 ‰) to be slightly to moderately altered and are most likely to archiving $\delta^{13}C$ signal and possibly the $\delta^{18}O$ values closest to the initial composition.

In Figure 24 $\delta^{13}C_{carb}$ the values of 15 samples which could be considered by criteria above as the least altered (all obtained from the centres of dolostone layers, $\delta^{18}O_{carb}$~–10 ‰, dolomite content >80 %wt) are displayed. In this case a positive $\delta^{13}C_{carb}$ trend from –4 to 0 ‰ can be observed through the sections. Melezhik and others (2015) studied two cores (12AB and 13A) which were taken from the same Zaonega Formation at about 70 km distance from OPH core. They found that carbon isotope signature in uppermost dolostone interval displays positive shift from –6 to –2 ‰ in dolostones presumably correlative to the beds studied in OPH core. Similar 4 ‰ shift towards positive $\delta^{13}C_{carb}$ values is observed in this study as well. However, Melezik and others (2015) also stated that this trend seems to be rather erratic and the samples which were considered least altered in this interval may still display significantly changed $\delta^{13}C_{carb}$ signature. To understand the true nature of the isotopic signal in Zaonega dolostones further studies are needed to reveal the origin of possibly different dolomite generations.

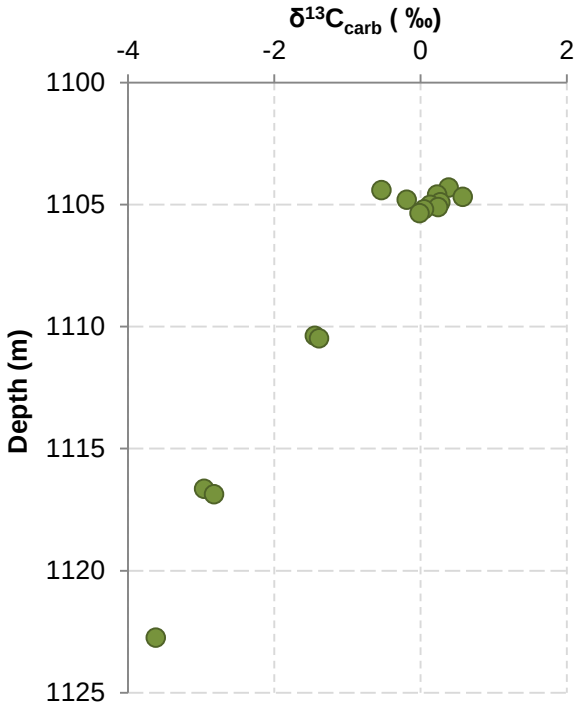

Figure 24. $\delta^{13}C_{carb}$ values which are considered least altered from their original value plotted along depth circles represent the values of $\delta^{18}O_{carb}$.

Conclusions

Carbon isotopic composition of carbonate rocks in the upper part of Zaonega Formation have been used in previous studies to reconstruct global environmental changes in Palaeoproterozoic era. Combined geochemical, mineralogical and petrographic observations of Zaonega carbonate rocks indicate that the primary sedimentary phase was most likely dolomite which was post-depositionally altered by at least three fluid-rock interaction episodes, casting a doubt in the applicability of previous studies concerning the primary isotope signature, because even in the central parts of the dolostone layers which have been previously considered as least altered may have been affected by fluid circulation episodes and may not preserve the isotopic signals of ambient sea-water.

The magnitude of $\delta^{13}C_{carb}$ depletion of calcite relative to dolomite is up to 17 ‰ and up to 10 ‰ for $\delta^{18}O_{carb}$ values. This magnitude can be explained by interaction between rock and a $\delta^{13}C$ and $\delta^{18}O$ depleted fluids carrying silica, resulting in precipitation of isotopically light secondary phases like calcite and possibly secondary dolomite as the latest phase. The formation of calcite is accompanied by dedolomitization, precipitation of authigenic quarz and different phyllosilicate minerals such as talc and mica. Post-depositional fluids, infiltrating the carbonates were possibly of magmatic or hydrothermal origin.

Carbonate rocks in studied interval are considerably affected by post-depositional alteration, therefore $\delta^{13}C_{carb}$ and $\delta^{18}O_{carb}$ cannot be used without careful screening as the proxy for primary depositional signature.

Acknowledgments

This study would not have been possible without samples collected by Kärt Üpraus, Timmu Kreitsmann, Sigrid Soomer and Kaarel Mänd. I am grateful to Jaan Aruväli who did not mind loads of sample preparations I secretly hoarded on his table, to Holar Sepp who taught what precision means, to Rait Kanarbik and Priit Möller for reaching impossible mass resolutions when needed.

References

Al-Aasm, I. S., Taylor, B. E., South, B., 1990. Stable isotope analysis of multiple carbon-ate samples using selective acid extraction. Chemical Geology, 80, 119–125.

Amelin, Y. V., Heaman, L. M., Semenov, V. S., 1995. U-Pb Geochronology of Layered Mafic Intrusions in the Eastern Baltic Shield – Implications for the Timing and Duration of Paleoproterozoic Continental Rifting. Precambrian Research, 75, 31–46.

Asael, D., Tissot, F. L. H., Reinhard, C. T., Rouxel, O., Dauphas, N., Lyons, T. W., Ponzevera, E., Liorzou, C., Chéron, S., 2013. Coupled molybdenum, iron and uranium stable isotopes as oceanic paleoredox proxies during the Paleoproterozoic Shunga Event. Chemical Geology, 362, 193–210.

Baker, A. J., Fallick, A. E., 1989a. Evidence from Lewisian limestones for isotopically heavy carbon in two-thousand-million-year-old sea water. Nature, 337, 352–354.

Baker, A. J., Fallick, A. E., 1989b. Heavy carbon in two-billion-year-old marbles from Lofoten-Vesterålen, Norway: implications for the Precambrian carbon cycle. Geochimica et Cosmochimica Acta, 53, 1111–1115.

Banner, J. L., Hanson, G. N., 1990. Calculation of simultaneous isotopic and trace element variations during water–rock interaction with applications to carbonate diagenesis. Geochimica et Cosmochimica Acta, 54, 3123–3137.

Bekker, A., Holland, H. D., Wang, P. L., Rumble, D. Stein, H. J., Hannah, J. L., Coetzee, L. L. Beukes, N. J., 2004. Dating the rise of atmospheric oxygen Nature, 427, 117-120.

Bekker, A., Karhu, J. A., Kaufman, A. J., 2006. Carbon isotope record for the onset of the Lomagundi carbon isotope excursion in the Great Lakes area, North America. Precambrian Research, 148, 145–180.

Benninghoven, A., Rüdenauer, F. G., Werner, H. W., 1987. Basic Concepts, Instrumental Aspects, Applications, and Trends, Wiley, New York.

Breecker, D. O., Payne, A. E., Quade, J., Banner, J. L., Ball, C. E., Meyer, K. W., Cowan, B. D., 2012. The sources and sinks of CO2 in caves under mixed woodland and grassland vegetation. Geochimica et Cosmochimica Acta, 96, 230–246.

Buick, I. S., Uken R., Gibson, R. L., Wallmach, T., 1998. High-$\delta^{13}C$ Paleoproterozoic carbonates from the Transvaal Supergroup, South Africa. Geological Society of America, 26-10, 875-878.

Burdett, J. W., Grotzinger, J. P., Arthur, M. A., 1990. Did Major Changes in the Stable-Isotope Composition of Proterozoic Seawater Occur? Geology, 18(3), 227-230.

Campbell, K. A., 2006. Hydrocarbon seep and hydrothermal vent palaeoenvironments and palaeontology: past developments and future research directions. Palaeogeography, Palaeoclimatology, Palaeoecology, 232, 362 – 407.

Crick, I. H., Boreham, C. J., Cook, C. A., Powell, T. G., 1988. Petroleum geology and geochemistry of middle Proterozoic McArthur basin, northern Australia: II. assessment of source rock potential. American Association of Petroleum Geologists Bulletin, 72, 1495–1514.

Črne, A. E., Melezhik, V. A., Lepland, A., Fallick, A. E., Prave, A. R., Brasier, A. T. 2014. Petrography and geochemistry of carbonate rocks of the Paleoproterozoic Zaonega Formation, Russia: Documentation of 13C-depleted non-primary calcite. Precambrian Research, 240, 79–93.

Črne, A. E., Melezhik, V. A., Prave, A. R., Lepland, A., Romashkin, A. E., Rychanchik, D. V., Hanski, E. J., 2013a. Zaonega Formation: FAR-DEEP Holes 12A and 12B, and Neighbouring quarries, in Melezhik, V. A., Prave, A. R., Fallick, A. E., Hanski, E. J., Lepland, A., Kump, L. R., and Strauss, H., eds., Reading the Archive of Earth's Oxygenation: The Core Archive of the Fennoscandian Arctic Russia - Drilling Early Earth Project, Volume 2, Springer, 946-1007.

Črne, A. E., Melezhik, V. A., Prave, A. R., Lepland, A., Romashkin, A. E., Rychanchik, D. V., Hanski, E. J., and Luo, Z., 2013b. Zaonega Formation: FAR-DEEP Hole 13A, in Melezhik, V. A., Prave, A. R., Fallick, A. E., Hanski, E. J., Lepland, A., Kump, L. R., and Strauss, H., eds., Reading the Archive of Earth's Oxygenation: The Core Archive of the Fennoscandian Arctic Russia - Drilling Early Earth Project, Volume 2, Springer, 1008-1046.

Derry, L. A., 2010. A burial diagenesis origin for the Ediacaran Shuram-Wonoka carbon isotope anomaly. Earth Planet Science Letters, 294, 152-162.

Des Marais, D. J., Strauss, H., Summons, R. E., Hayes, J. M., 1992. Carbon isotope evidence for the stepwise oxidation of the Proterozoic environment. Nature, 359, 605–609.

Friedman, I., O'Neil, J. R., 1977: Compilation of stable isotope fractionation factors of geochemical interest, in: Data of Geochemistry 6th, Geological Survey professional paper, 440.

Frisia S., Fairchild, I. J., Fohlmeister, J., Miorandi, R., Spötl, C., Borsato, A., 2011. Carbon mass-balance modelling and carbon isotope exchange processes in dynamic caves. Geochimica et Cosmochimica Acta, 75, 380-400.

Glushanin, L. V., Sharov, N. V., Shchiptsov, V. V., 2011. Palaeoproterozoic onega structure (geology, tectonics, deep structure and mineralogeny). Karelian research centre, Petrozavotsk, 431 (in Russian).

Hannah, J. L., Stein, H., Yang, G., Zimmerman, A., Melezhik, V., Filippov, M., Turgeon, S., Creaser, R., 2008. Re-Os geochronology of a 2.05 Ga fossil oil field near Shunga, Karelia, NW Russia, the 33rd International Geological Congress, Oslo, Norway

Hayes, J. M., Waldbauer, J. R., 2006. The carbon cycle and associated redox processes through time. Philosophical Transactions of the Royal Society B, 361:931–950.

Holland, H. D., 2004. The geological history of seawater. In: Holland, H. D., Turekian, K. K. (eds) Treatise on Geochemistry. Elsevier, Oxford, 6, 583–625.

Ivankin, P. F., Galdobina, L. P., Kalinin, Yu. K., 1987. Shungites: origin and classification of a new carbon mineral resource. International Geology Review, 29, 1208–1214.

Jacobsen, S. B., Kaufman, A. J., 1999. The Sr, C and O isotopic evolution of Neoproterozoic seawater. Chemical Geology, 161, 37– 57.

Karhu, J. A., Holland, H. D., 1996. Carbon isotopes and the rise of atmospheric oxygen: Geology, 24-10, 867-870.

Karhu, J.A., 1993. Paleoproterozoic evolution of the carbon isotope ratios of sedimentary carbonates in the Fennoscandian Shield: Espoo. Geological survey of Finland bulletin, 371-87.

Kaufman, A. J., Knoll, A. H., 1995. Neoproterozoic variations in the C-isotopic composition of seawater: stratigraphic and biogeochemical implications. Precambrian Research, 73, 27–49.

Knauth, L. P., Kennedy, M. J., 2009. The late Precambrian greening of the Earth. Nature, 460, 728–732.

Knoll, A. H., Hayes, J. M., Kaufman, A. J., Swett, K., Lambert, I. B., 1986. Secular variation in carbon isotope ratios from upper Proterozoic successions of Svalbard and East Greenland. Nature, 321, 832–838.

Krupenik, V. A., Akhmedov, A. M., Sveshnikova, K. Y., 2011. Isotopic composition ofcarbon, oxygen and sulphur in the Ludicovian and Jatulian rocks. In: Glushanin, L. V., Sharov, N. V., Shchiptsov, V. V. (Eds.), Palaeoproterozoic Onega Structure (Geology, Tectonics, Deep Structure and Mineralogeny). Karelian Research Cen-tre, Russian Academy of Sciences, Petrozavodsk, 250–255 (in Russian).

Kump, L. R., Junium, C., Arthur, M. A., Brasier, A., Fallick, A., Melezhik, V., Lepland, A., Črne, A. E., Luo G., 2011. Isotopic Evidence for Massive Oxidation of Organic Matter Following the Great Oxidation Event. Science, 334, 1694-1696.

Lyons, T. W., Reinhard, C. T., Planavsky, N. J., 2014. The rise of oxygen in Earth's early ocean and atmosphere. Nature, 506, 307–315.

Martin, A. P., Condon, D. J., Prave, A. R., Melezhik, V. A., Lepland, A., Fallick, A. E., 2013. Dating the termination of the Palaeoproterozoic Lomagundi-Jatuli carbon isotopic event in the North Transfennoscandian Greenstone Belt. Precambrian Research, 224, 160–168.

Martin, A. P., Prave, A. P., Condon, D. J., Lepland, A., Fallick, A. E., Romashkin, A. E., Medvedev, P. V., Rychanchik, D. V., 2015. Multiple Palaeoproterozoic Carbon Burial Episodes and Excursions. Earth and Planetary Science Letters, 424, 226–236.

Melezhik, V. A., Fallick, A. E., Filippov, M. M., Larsen, O., 1999. Karelian shungite an indication of 2.0-Ga-old metamorphosed oil-shale and generation of petroleum: geology, lithology and geochemistry. Earth-Science Reviews, 47, 1–40.

Melezhik, V. A., Fallick, A. E., Smirnov, Y. P., Yakovlev, Y. N., 2003. Fractionation of carbon and oxygen isotopes in ^{13}C-rich Palaeoproterozoic dolostones in the transition from medium-grade to high-grade greenschist facies: a case study from the Kola Superdeep Drillhole. Journal of the Geological Society, 160, 71–82

Melezhik, V. A., Filippov, M. M., Romashkin, A. E., 2004. A giant Palaeoproterozoic deposit of shungite in NW Russia: genesis and practical applications. Ore Geology Reviews, 24, 135–154

Melezhik, V. A., Hanski, E. J., 2013. The Pechenga Greenstone Belt, in: Melezhik, V. A., Prave, A. R., Hanski, E. J., Fallick, A. E., Lepland, A., Kump, L. R., Strauss, H. (Eds.), Reading the Archive of Earth's Oxygenation. Volume 1: The Paleoproterozoic of Fennoscandia as Context for the Fennoscandian Arctic Russia-Drilling Early Earth Project, 289–385.

Melezhik, V. A., Huhma, H., Condon, D. J., Fallick, A. E., Whitehouse, M. J., 2007. Temporal constraints on the Paleoproterozoic Lomagundi-Jatuli carbon isotopic event. Geology, 35, 655–658

Melezhik, V. A., Medvedev, P. V., Svetov, S. A., 2013. The Onega Basin, in: Melezhik, V. A., Prave, A. R., Hanski, E. J., Fallick, A. E., Lepland, A., Kump, L. R., Strauss, H. (Eds.), Reading the Archive of Earth's Oxygenation. Volume 1: The Paleoproterozoic of Fennoscandia as Context for the Fennoscandian Arctic Russia-Drilling Early Earth Project, 387-490.

Oehlert, A. M., Swart, P. K., 2014. Interpreting carbonate and organic carbon isotope covariance in the sedimentary record. Nature Communications, 5, 4672.

Ovchinnikova, G. V., Kuznetsov, A. B., Melezhik, V. A., Gorokhov, I. M., Vasil'eva, I. M., Gorokhovskii, B. M., 2007. Pb-Pb age of Jatulian carbonate rocks: The Tulomozero Formation of Southeast Karelia. Stratigraphy and Geological Correlation, 15, 359–372.

Premovic, P. I., Komatinovic, B. V., Pugmire, R. J., Woolfenden, W. R., 1988. Solid-state 13C NMR of middle Precambrian anthracite and related anthraxolite. Naturwissenschaften, 75, 98–100.

Puchtel, I. S., Brugmann, G. E., Hofmann, A. W., 1999. Precise Re-Os mineral isochron and Pb-Nd-Os isotope systematics of a mafic-ultramafic sill in the 2.0 Ga Onega plateau (Baltic Shield). Earth and Planetary Science Letters, 170, 447–461.

Qu, Y., Črne, A. E., Lepland, A., Van Zuilen, M. A., 2012. Methanotrophy in a Paleoproterozoic oil field ecosystem, Zaonega Formation, Karelia, Russia. Geobiology, 10, 467–478.

Romanek, C. S., Grossman, E. L., Morse, J. W., 1992. Carbon isotopic fractionation in synthetic aragonite and calcite: Effects of temperature and precipitation rate. Geochimica et Cosmochimica Acta, 56 (1), 419–430.

Sapart, C. J., Monteil, G., Prokopiou, M., van de Wal, R. S. W., Kaplan, J. O., Sperlich, P., Krumhardt, K. M., van der Veen, C., Houweling, S., Krol, M. C., Blunier, T., Sowers, T.,

Martinerie, P., Witrant, E., Dahl-Jensen, D., Röckmann, T., 2012. Natural and anthropogenic variations in methane sources during the past two millennia. Nature, 490, 85–88.

Schidlowski, M., 2001. Carbon isotopes as biogeochemical recorders of life over 3.8 Ga of Earth history: Evolution of a concept. Precambrian Research, 106, 117–134.

Sheppard, S. M. F., 1986. Characterization and isotopic variations in natural waters. Reviews in mineralogy, 16, 165-183.

Strauss, H., Des Marais, D. J., Hayes, J. M., Summons, R. E., 1992. The carbon-isotopic record. In: Schopf, J. W., Klein, C. eds., The Proterozoic Biosphere: A Multidisciplinary Study. Cambridge University, 117–127.

Strauss, H., Melezhik, V. A., Lepland, A., Fallick, A. E., Hanski, E. J., Filippov, M. M., Deines, Y. E., Illing, C. J., Črne, A. E., Brasier, A. T., 2013. 7. 6 Enhanced accumula-tion of organic matter: the Shunga event. In: Melezhik, V. A., Kump, L. R., Fallick, A. E., Strauss, H., Hanski, E., Prave, A. R., Lepland, A. (eds.), Reading the Archive of Earth's Oxygenation, vol. 3. Springer, Berlin Heidelberg, 1195–1273.

Swanson-Hysell, N. L., Rose, C. V., Calmet, C. C., Halverson, G. P., Hurtgen, M. T., Maloof, A. C., 2010. Cryogenian glaciation and the onset of carbon-isotope decoupling. Science, 328, 608–611.

Valley, J. W., 1986. Stable isotope geochemistry of metamorphic rocks. In: Valley, J. W., Taylor, H. P., O'Neil, J. R. (eds) Stable Isotopes in High Temperature Geological Processes. Mineralogical Society of America, Reviews in Mineralogy, 16, 445–489.

Whiticar, M. J., 1999. Carbon and hydrogen isotope systematics of bacterial formation and oxidation of methane. Chemical Geology, 161, 291–314.

Üpraus, K., 2014. Chert-dolostone sequences in Zaonega Formation, Karelia: implication to the chert origin. MSc thesis, University of Tartu.

Yudovich, Y. E., Makarikhin, V. V., Medvedev, P. V., Sukhanov, N. V., 1991. Carbon isotope anomalies in carbonates of the Karelian Complex. Geochemica International, 28, 56–62.

Sekundaarsed muutused Paleoproterosoikumi Zaonega kihistu karbonaatsetes kivimites Onega parameetrilises puuraugus, Karjalas Venemaal

Marian Külaviir

Kokkuvõte

Karbonaatsete kivimite isotoopset koostist Zaonega kihistus on laialdaselt uuritud Paleoproterosoikumi süsinikuringe rekonstrueerimiseks kuid Zaonega kihistu kivimite algne isotoopne koostis on oluliselt mõjutatud fluidide ja moondeprotsesside poolt, seetõttu on globaalsete keskkonnamuutuste väljaselgitamisel oluline eristada karbonaatkivimite algset ja sekundaarset isooopkoostist. Käesoleva töö eesmärgiks on Onega parameetrilise puuraugu Zaonega kihistu ülemise osa karbonaatkivimite mineraloogilise ja isotoopse koostise kirjeldamine, sekundaarsete protsesside, nende mehhannismide ja ulatuse esile toomine ning võimalikult primaarse isotoopsignaali leidmine uuritavas intervallis. Mineraloogiliste, petrograafiliste ja geokeemiliste analüüside tulemusena leiti, et karbonaatsete kivimikihtide keskosas on domineerivaks mineraaliks dolomiit ning kihtide äärealadel kaltsiit, kusjuures kaltsiit on võrreldes dolomiidiga nii ^{13}C-st kui ka ^{18}O-st vaesustunud. Vaesustumine on toimunud sekundaarsetes protsessides mille käigus isotoopselt kerged, räinidioksiidi sisaldavad magmalised või hüdrotermaalsed fluidid reageerisid karbonaatse kivimiga. Fluidi ja kivimi vastasmõjul tekkisid ^{13}C-ja ^{18}O-vasustunud sekundaarsed karbonaatsed faasid. Kõige tõenäolisemalt olid ^{13}C-vaesed ühendid pärit orgaanilise materjali lagunemisest/oksüdeerumisest. Ränidioksiidi ja dolomiidi reaktsioonil tekkisid kaltsiit, autigeenne kvarts ja kihtsilikaadid, neid mineraale on kõige rohkem näha karbonaatkivimi kihtide äärtel. Võrreldes $\delta^{13}C_{carb}$ ja $\delta^{18}O_{carb}$ graafikut Jacobseni ja Kaufmani (1999) masstasakaalu mudeliga on näha, et peale settimist on Zaonega kihistu karbonaatkivimid erineva koostisega fluididega reageerinud vähemalt kolmel erineval korral. Karbonaatsed kivimid uuritavas intervallis on tugevasti moonutatud oma algse isotoopkoostise suhtes ning seetõttu tuleb primaarse isotoopsignatuuri kirjeldamisel hoolikalt kaaluda kõiki võimalikke hilisemaid hüdrotermaal- ja moondeprotsesse mis võisid isotoopsignatuuri mõjutada.

Appendix

Table 1. Depth and mineralogy of the samples

Depth(m)	Quartz(%)	K-feldspar(%)	Albite(%)	K/Mg-mica(%)	Talc(%)	Chlorite(%)	Pyrite(%)	Apatite(%)	Calcite(%)	Dolomite(%)	Siderite(%)
1103.59	14.8	0.6	0.4	7.4			0.4	1.2	73.8	1.3	
1103.61	25.5	2.5		8.2			0.5	1.3	60.0	1.9	
1103.64	6.6	1.0	0.5	2.8			0.5	0.5	23.3	64.9	
1103.74	27.5	0.4	0.2	6.4			0.3	0.6	61.1	3.5	
1103.93	27.1	1.2	0.3	6.4			0.6	0.5	24.3	39.6	
1104.03	7.4	1.0	0.7	3.9	1.1		0.4	0.5	10.2	74.9	
1104.115	4.7	1.0	0.6	2.6			0.4		14.9	75.7	
1104.215	33.7	1.5	0.6	8.2			0.4	1.5	48.4	5.7	
1104.31	0.7	1.7	0.8	3.0			0.3	0.5	5.2	87.6	
1104.41	0.8	1.4	1.0	2.6		0.9		0.2	3.5	89.4	
1104.6	1.9	1.5	1.9	3.5			0.3	0.7	7.3	82.9	
1104.69	0.4	1.4	0.7	2.4			0.3	0.6	11.0	83.2	
1104.8	0.5	0.5		2.4			0.3	0.7	2.2	92.6	0.7
1104.91	0.6	1.2	1.3	3.3			0.3	1.0	1.6	90.7	
1105.01	1.0	1.2	0.9	3.7			0.3	0.7	2.1	89.5	0.5
1105.11	0.6	1.0	0.7	2.6				0.3	1.8	92.7	0.2
1105.2	1.0	1.0	0.7	1.8		0.6	0.4		4.0	90.5	
1105.36	0.5	0.9	0.7	2.5			0.4		2.6	92.4	
1105.46	0.2	1.1	0.4	2.5			0.5		10.5	84.9	
1105.55		1.6	0.5	2.5			0.3		8.6	86.3	
1105.67		2.0	1.1	3.4			0.2	0.6	9.2	83.4	
1105.77	0.2	1.2	0.7	3.2			0.2	0.7	5.3	88.6	
1105.91	0.2	1.1	0.7	4.0			0.3	0.3	7.4	86.0	
1106.01	0.4	1.9	0.5	5.0	2.0		0.2	0.5	10.3	79.2	
1106.1	0.4	1.9	0.9	5.3	1.5		0.4	1.2	14.2	74.1	

Depth(m)	Quartz(%)	K-feldspar(%)	Albite(%)	K/Mg-mica(%)	Talc(%)	Chlorite(%)	Pyrite(%)	Apatite(%)	Calcite(%)	Dolomite(%)	Siderite(%)
1106.21	0.4	1.5	0.8	4.4	1.4		0.6		21.2	69.6	
1106.31		1.2	0.3	3.4			0.2		2.9	91.9	
1106.43	0.5	0.8	0.8	6.0	1.0		0.5	0.2	5.2	84.9	
1106.53	0.3	1.9	1.0	4.2	1.9		0.5	0.2	13.8	76.3	
1106.63	3.8	0.7	1.1	9.4	6.9		0.4	0.9	54.7	22.1	
1106.74	4.5	0.5	1.5	14.4	15.8		1.6	0.4	42.8	18.4	
1106.8	7.8	1.5	0.6	7.4			0.9	1.3	76.4	4.0	
1106.82	3.7	0.9		8.2			0.8	1.2	83.0	2.0	
1106.84	5.9	1.2	1.0	10.5			0.9	1.7	77.1	1.5	
1107.76	16.3	0.2		12.9			0.7	0.6	69.0	0.4	
1107.78	27.8	1.2	0.2	10.6			0.5	1.2	56.8	1.7	
1107.81	4.1	1.1	0.6	2.0			0.3		5.4	86.6	
1107.87	13.1	0.2	0.4	21.1					59.2	5.8	
1107.79	21.7	1.8	0.4	12.6			0.8	1.0	51.8	9.9	
1107.89	4.7	1.4	0.5	3.3					6.9	83.0	
1108.06	3.8	1.5	0.6	2.6					6.9	84.5	
1108.14	4.0	1.0	1.1	2.3			0.2	0.2	11.6	79.6	
1108.23	9.0	1.9	0.9	4.3			0.2	0.6	48.7	34.5	
1108.3	8.3	0.5	0.3	19.7				0.5	43.8	26.9	
1108.52	5.1	1.5	0.6	5.1				0.2	24.6	62.9	
1108.54	1.5	0.9	0.5	3.5			0.4		11.6	81.6	
1108.57	1.3	0.6	0.6	2.4					1.2	93.6	
1108.67	1.6	0.8	1.0	2.8					2.4	91.3	
1108.77	1.0	1.5	0.8	2.5				0.2	12.0	81.9	
1108.9	2.6	1.8	1.1	2.9	1.4		0.2	0.3	10.5	79.3	
1109.02	0.6	2.0	0.8	2.7	1.1		0.4	0.3	19.5	72.6	
1109.12	1.8	1.4	0.7	2.1	0.4		0.2		6.3	87.1	
1109.23	6.0	1.9	0.9	2.3				0.2	7.7	81.0	
1109.33	22.4	2.6	0.5	5.8			0.6	0.4	30.8	36.9	

Depth(m)	Quartz(%)	K-feldspar(%)	Albite(%)	K/Mg-mica(%)	Talc(%)	Chlorite(%)	Pyrite(%)	Apatite(%)	Calcite(%)	Dolomite(%)	Siderite(%)
1109.42	5.8	2.0	0.5	4.9					1.8	84.8	
1109.57	10.1	2.0	0.4	4.2	1.0			1.4	3.9	76.9	
1109.66	2.1	1.0	0.8	3.2	1.6			3.4	1.9	86.0	
1109.76	0.9	1.4	0.6	4.2	3.2		0.2	0.2	14.6	74.8	
1109.86	0.5	1.0	0.6	2.0	1.5		0.2	3.9	11.8	78.4	
1109.96	0.2	1.4	0.6	3.4	1.3		0.3	0.5	12.4	79.8	
1110.06	0.6	1.4	0.5	3.9			0.3	4.1	10.3	78.9	
1110.14	0.4	1.0	0.6	5.9	2.5			0.3	10.8	78.5	
1110.24	0.3	0.9	0.5	4.3	1.7			4.3	9.0	79.0	
1110.38	0.9	1.5	0.3	2.8	2.0			2.5	10.4	79.5	
1110.48		0.8	0.5	1.5	0.8		0.3	0.5	8.5	87.0	
1110.56	0.3	1.3	0.2	1.9	1.0		0.3	0.6	9.3	85.2	
1110.66	0.2	1.4	0.4	2.6			0.3	0.4	4.7	90.0	
1110.75	0.2	0.7	0.6	3.4			0.2	0.2	8.9	85.9	
1110.89	0.3	1.9	0.6	4.2	2.1		0.2		13.8	76.9	
1111.06	3.0	1.9	0.7	4.1	1.5		0.5	0.4	32.3	55.7	
1111.16	0.9	1.9	0.2	3.9	2.3				11.0	79.7	
1111.25	1.0	1.7	0.5	3.8	3.2		0.2		9.2	80.2	
1111.39	1.3	1.7	0.5	4.9	3.1				3.5	85.0	
1111.6	1.0	2.4	0.4	4.8	3.1			3.8	5.5	78.9	
1111.7	1.1	1.8	0.7	3.6	1.5		0.4	0.6	19.6	70.8	
1111.8	3.2	1.5	0.6	6.7	3.4		0.2	6.1	13.3	64.9	
1111.83	2.4	1.6	1.3	10.6	11.7		0.7		30.8	40.4	0.4
1111.92	6.4	2.1	0.3	7.0			0.7	1.2	50.5	31.8	
1111.97	10.2	1.4	0.4	11.7			1.3	1.1	67.9	5.9	
1111.99	10.1	2.4	0.6	52.4			0.9		31.6	1.7	0.4
1115.43	28.0	0.9		33.1			0.8		36.1	0.7	0.4
1115.45	44.6	0.5		7.4			1.2	0.3	45.0	1.0	
1115.5	3.9	2.0	0.2	2.7			1.0	0.2	12.4	77.8	

Depth(m)	Quartz(%)	K-feldspar(%)	Albite(%)	K/Mg-mica(%)	Talc(%)	Chlorite(%)	Pyrite(%)	Apatite(%)	Calcite(%)	Dolomite(%)	Siderite(%)
1115.6	6.8	1.8	0.4	2.9			1.7	0.2	8.3	77.9	
1115.68	1.6	1.0	0.2	1.8			0.5		9.8	85.1	
1115.78	10.2	1.9	0.3	3.7			0.4	0.3	22.2	61.1	
1115.81	5.6	1.1		9.7			0.7	1.4	79.3	2.0	
1115.83	2.6	2.9	2.2	86.7			1.4		2.9	1.0	0.4
1115.98	7.2	2.7	1.0	70.4			1.8	0.2	15.1	1.3	0.3
1116	11.9	1.2	0.3	3.9	3.6		2.1	0.4	24.7	52.0	
1116.05	3.5	1.4	0.3	2.9	1.9		0.8	0.5	3.8	84.9	
1116.14	12.7	1.8	0.5	18.8			1.3		6.9	57.9	
1116.27	2.5	1.1	0.3	4.5	6.0		1.5		8.0	76.2	
1116.37	1.3	2.2	0.4	9.3	7.3		2.5		6.8	70.1	
1116.46	0.2	0.8	0.4	4.3	1.9		0.9		1.8	89.6	
1116.56	0.2	1.1	0.3	4.1			0.7		4.1	89.5	
1116.65	0.6	1.3	0.3	2.8			0.6		4.7	89.6	
1116.77	4.8	1.3	0.4	3.2			0.3		8.8	81.2	
1116.87	0.4	1.2	0.5	2.5	2.0		0.4		2.2	90.8	
1116.96	0.3	1.7	0.8	6.2	2.3		1.0	0.2	1.1	86.5	
1117.07	0.5	1.3	0.4	4.1	0.9		1.5		3.7	87.5	
1117.17	0.9	1.5	0.7	4.8	2.0		0.9	0.5	3.2	85.5	
1117.27	1.9	1.5	0.7	4.2	1.2		0.7	0.5	3.8	85.4	
1117.37	10.4	0.9	0.3	5.0			1.1	0.2	4.1	78.1	
1117.41	23.6	0.8	0.4	10.7			5.4	0.6	53.0	5.5	
1122.33	1.6	3.4	1.0	60.9		2.8	2.0	0.4	25.9	1.7	0.4
1122.42	3.0	1.4	0.6	6.1			1.6		13.6	73.7	
1122.53	6.6	2.0		7.5			3.9	1.2	76.5	2.2	
1122.65	1.6	1.0	0.6	3.1			1.6		12.5	79.4	
1122.75	0.5	0.8	0.3	5.0			1.4	0.3	11.0	80.7	
1122.85	0.6	1.3	0.4	5.9			4.5	0.2	8.0	79.2	
1122.96	11.5	1.5	0.6	5.6			3.4		9.9	67.5	

Depth(m)	Quartz(%)	K-feldspar(%)	Albite(%)	K/Mg-mica(%)	Talc(%)	Chlorite(%)	Pyrite(%)	Apatite(%)	Calcite(%)	Dolomite(%)	Siderite(%)
1123.03	14.4	2.5	0.3	9.5			4.2	1.1	39.3	28.7	
1123.13	17.1	1.2	0.4	10.4			5.7	1.4	62.3	1.5	
1123.18	52.7	1.8	1.0	22.5			10.7	0.2	10.7	0.3	
1123.2	32.15	3.06	2.66	52.48			7.51	0.03	1.63	0.38	

Table 2. Depth and isotopic composition of samples

Depth (m)	$\delta^{13}C_{carb}$(‰)	$\delta^{18}O_{carb}$(‰)	$\delta^{13}C_{org}$(‰)	Depth (m)	$\delta^{13}C_{carb}$(‰)	$\delta^{18}O_{carb}$(‰)	$\delta^{13}C_{org}$(‰)
1103.59	-8.88	-14.89	-35.84	1108.23	-7.92	-12.90	-36.25
1103.61	-15.58	-15.09		1108.3	-7.90	-12.55	
1103.64	-5.23	-12.72		1108.52	-5.34	-9.51	
1103.74	-12.61	-14.97		1108.54	-5.05	-9.10	-35.97
1103.93	-6.15	-12.54	-36.27	1108.57	-4.98	-8.90	
1104.03	-3.29	-7.07		1108.67	-4.57	-12.02	
1104.115	-4.64	-10.47	-35.87	1108.77	-5.00	-11.93	-36.15
1104.215	-13.21	-14.51	-35.84	1108.9	-4.17	-11.35	
1104.31	0.39	-10.08		1109.02	-3.89	-10.99	
1104.41	-0.53	-11.53	-26.30	1109.12	-3.93	-10.81	-35.79
1104.6	0.23	-8.77	-26.01	1109.23	-3.72	-10.41	
1104.69	0.58	-9.32	-24.30	1109.33	-7.74	-12.46	
1104.8	-0.19	-11.59	-24.62	1109.42	-2.25	-4.79	-36.52
1104.91	0.27	-10.07	-25.14	1109.57	-4.27	-7.21	
1105.01	0.13	-10.23	-25.13	1109.66	-2.42	-5.76	
1105.11	0.24	-11.08	-25.78	1109.76	-4.33	-12.54	-36.08
1105.2	0.05	-10.90	-25.05	1109.86	-2.49	-12.36	
1105.36	-0.01	-10.17	-24.38	1109.96	-1.86	-12.33	
1105.46	-1.37	-11.40	-33.32	1110.06	-1.92	-12.02	-35.31
1105.55	-1.99	-11.08	-33.32	1110.14	-2.41	-11.72	
1105.67	-2.02	-11.28	-32.61	1110.24	-2.09	-11.71	
1105.77	-2.82	-9.40	-34.02	1110.38	-1.44	-11.99	-35.54
1105.91	-3.79	-9.44	-32.78	1110.48	-1.39	-11.41	
1106.01	-4.47	-9.87		1110.56	-2.58	-10.89	
1106.1	-4.05	-10.10	-35.06	1110.66	-3.26	-10.17	-36.72
1106.21	-5.69	-10.50		1110.75	-3.77	-10.90	
1106.31	-3.72	-7.06		1110.89	-5.63	-11.76	
1106.43	-4.64	-7.13	-34.81	1111.06	-6.80	-12.84	-36.53
1106.53	-4.44	-9.38		1111.16	-4.92	-11.71	
1106.63	-8.38	-14.15		1111.25	-6.44	-11.67	
1106.74	-9.89	-14.21	-34.65	1111.39	-6.18	-11.43	-36.52
1106.8	-11.62	-14.92		1111.6	-7.65	-11.63	
1106.82	-9.38	-15.17		1111.7	-8.48	-12.16	
1106.84	-7.07	-15.08	-34.73	1111.8	-6.64	-12.39	-36.55
1107.76	-12.69	-15.08	-36.26	1111.83	-8.30	-13.16	
1107.78	-16.87	-14.98		1111.92	-8.41	-13.63	
1107.81	-4.58	-10.80	-35.85	1111.97	-10.19	-14.63	
1107.87	-14.85	-14.72		1111.99	-11.13	-14.88	-36.55
1107.79	-12.26	-14.24		1115.43			
1107.89	-3.86	-11.29	-35.82	1115.45	-11.11	-14.87	-36.87
1108.06	-5.07	-11.09		1115.5	-6.48	-11.75	
1108.14	-5.28	-11.22		1115.6	-4.97	-8.86	

Depth (m)	$\delta^{13}C_{carb}$(‰)	$\delta^{18}O_{carb}$(‰)	$\delta^{13}C_{org}$(‰)
1115.68	-5.34	-11.59	-36.68
1115.78	-6.55	-12.77	
1115.81	-12.04	-14.98	-36.75
1115.83			
1115.98	-12.24	-14.79	
1116	-7.44	-11.58	
1116.05	-4.75	-9.89	-37.12
1116.14	-7.38	-10.07	
1116.27	-7.58	-10.75	
1116.37	-7.91	-11.12	-37.20
1116.46	-6.26	-10.00	
1116.56	-4.18	-10.23	
1116.65	-2.96	-9.17	-36.94
1116.77	-6.26	-9.39	
1116.87	-2.82	-8.53	
1116.96	-5.59	-8.87	-37.13
1117.07	-4.17	-8.55	
1117.17	-5.00	-8.31	
1117.27	-6.45	-8.85	-37.13
1117.37	-9.53	-10.02	
1117.41	-10.49	-13.99	-37.47
1122.33	-10.67	-14.78	-36.04
1122.42	-5.81	-11.26	
1122.53	-11.02	-14.76	
1122.65	-4.36	-11.27	-35.74
1122.75	-3.62	-10.46	
1122.85	-4.17	-10.08	
1122.96	-8.84	-11.77	-36.63
1123.03	-9.36	-13.30	
1123.13	-9.22	-14.59	
1123.18	-11.26	-14.26	-35.96

Non-exclusive licence to reproduce thesis and make thesis public

I, _____Marian Külaviir _____,

(*author's name*)

1. herewith grant the University of Tartu a free permit (non-exclusive licence) to:

1.1. reproduce, for the purpose of preservation and making available to the public, including for addition to the DSpace digital archives until expiry of the term of validity of the copyright, and

1.2. make available to the public via the web environment of the University of Tartu, including via the DSpace digital archives until expiry of the term of validity of the copyright,

___Secondary changes in Palaeoproterozoic Zaonega Formation carbonate rocks in Onega Parametric Hole, Karelia, Russia_____,

(*title of thesis*)

supervised by _____Kalle Kirsimäe and Aivo Lepland__ _____,

(supervisor's name)

2. I am aware of the fact that the author retains these rights.

3. I certify that granting the non-exclusive licence does not infringe the intellectual property rights or rights arising from the Personal Data Protection Act.

Tartu, **20.05.2016**